# Accepted Manuscript

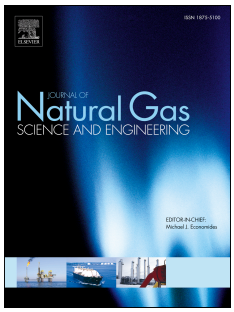


Micromechanical investigation of fines liberation and transport during coal seam dewatering

Travis R. Mitchell, Christopher R. Leonardi

PII: S1875-5100(16)30678-3

DOI: 10.1016/j.jngse.2016.09.038

Reference: JNGSE 1814

To appear in: *Journal of Natural Gas Science and Engineering*

Received Date: 29 March 2016

Revised Date: 8 September 2016

Accepted Date: 13 September 2016

Please cite this article as: Mitchell, T.R., Leonardi, C.R., Micromechanical investigation of fines liberation and transport during coal seam dewatering, *Journal of Natural Gas Science & Engineering* (2016), doi: 10.1016/j.jngse.2016.09.038.

# Micromechanical investigation of fines liberation and transport during coal seam dewatering

Travis R. Mitchell[a], Christopher R. Leonardi[a,b]

[a]*School of Mechanical and Mining Engineering, The University of Queensland The University of Queensland, Brisbane QLD 4072, Australia*
[b]*Department of Civil and Environmental Engineering, Massachusetts Institute of Technology*
*77 Massachusetts Avenue, Cambridge, MA 02139, USA*

## Abstract

The reduction of subsurface hydrostatic pressure to allow natural gas desorption is an integral step in the production of coal seam gas (CSG). During this dewatering stage, viscous stresses can cause the liberation and transport of fines, which are predominantly comprised of inorganic clay groups such as smectite, illite and kaolin, from within the coal matrix. Dislodged particles migrate in production fluid through fractures towards the wellbore where capture and deposition can deteriorate the reservoir's permeability. Once in the wellbore, these particles can adversely affect the performance of mechanical equipment such as pumps. This study uses direct numerical simulation of a synthetic coal fracture to help elucidate the particle detachment process. This is approached using a coupled lattice Boltzmann-discrete element method to capture both physical and physicochemical interactions based on Derjaguin-Landau-Verwey-Overbeek (DLVO) theory. Preliminary testing with the developed model suggests that particles move almost freely along the bounding surface regardless of electrostatic interactions, and that Hele-Shaw predictions of particle lift in particular can be inadequate. Further, larger-scale simulations indicated that the DLVO parameters can significantly impact the vertical position of propagating fines with variations in eroded mass of over 100% observed for the range of tested salinity levels.

*Keywords:* Fines migration, detachment kinetics, DLVO interactions, lubrication forces, lattice Boltzmann method, discrete element method

*Email addresses:* t.mitchell@uq.edu.au (Travis R. Mitchell), c.leonardi@uq.edu.au, chrisleo@mit.edu (Christopher R. Leonardi)

## 1. Introduction

In the production of coal seam gas (CSG) a common phenomenon causing reduced gas extraction and damage to upstream equipment is the detachment and migration of fine particles from within the coal seam. These particles have been observed in laboratory and field tests to have the potential to reduce coal seam permeability and induce what is referred to as formation damage. The transport of solids to the surface can also cause premature failure of pumps and piping equipment, leading to excessive wear and loss of containment in extreme cases. The processes by which fines are detached is yet to be fully understood (Bradford and Torkzaban, 2008) and mitigation tactics are yet to be proven completely effective. This investigation aims to numerically model the detachment process in order to further develop an understanding of the migration phenomenon.

In order to extract CSG, drilling operations are performed which allow ground water to be pumped to the surface. It is during this dewatering stage that particle detachment and transport towards the wellbore is investigated. Fine particles, herein referred to as fines, are defined in this study as clay particles able to be suspended in production fluid, and have sizes on the order of micrometers. Whilst research into the phenomenon of particle detachment and migration in CSG exists, the majority of these studies tend to be limited to continuum models in which concentration levels of suspended particles are tracked through advective-diffusive transport equations (Bradford et al., 2003; Bedrikovetsky et al., 2011; Zeinijahromi et al., 2012). In comparison, this study will focus on the grain-scale interactions that result in particle liberation.

The permeability of coal is an important parameter when considering CSG extraction. The transportation of methane towards the surface involves two stages. It first diffuses from the coal matrix before flowing through macropores in the coal seam towards a wellbore. The macropores include the network of face and butt cleats, bedding planes, and any other natural or induced fractures. In the most straightforward scenario the bedding planes are oriented perpendicular to gravity, however this can change post-deposition due to large-scale strata movement (e.g. faulting, folding). The face cleats are then typically parallel to the bedding planes and the butt cleats orthogonal to both. For the most part, it is these fractures that facilitate extraction which is economically feasible. Therefore, when these flow channels reduce in size and or become blocked production is often adversely affected.

When discussing the migration of fines in this report, reference is being given to the entire sequence of occurrences that determine their trajectory through the reservoir as well as their final capture or extraction. This includes foremost the detachment and or release behaviour of fines from the porous matrix. Khilar and Fogler (1998) reported the detachment of fines to be a result of colloidal interaction (both with the surface and additional migratory fines) and hydrodynamic forces, which are directly simulated in this investigation.

This paper presents a numerical framework for the simulation of grain-scale interactions that act to detach and transport fines within a coal seam. The developed computational model employs the lattice Boltzmann method (LBM) to replicate fluid flow coupled with the discrete element method (DEM) to track the behaviour of fines. Section 2 briefly reviews the physicochemical forces that act on fines along with empirical models for detachment kinetics. The direct numerical simulation (DNS) approach employed in this study is presented in Section 3, including the DEM for particle mechanics, the LBM for fluid mechanics, and the implementation, validation and verification of physicochemical particle forces. Section 4 summarises the results of small-scale simulations that investigate the liberation and transport of fines and, finally, Section 5 offers some concluding remarks.

## 2. Modelling of Fines as Colloids

In this study, fines are modelled as spherical colloidal particles. In doing this, the charge and average size of each particle can be defined in order to analyse its behaviour under varying subsurface environmental conditions. Thus, as particles are detached from the coal matrix a particle suspension problem is formed. This can have an impact on the rheology of the fluid in the system, and as such an understanding of how detachment occurs is necessary.

### *2.1. Colloidal Interactions*

Colloid mobilisation and immobilisation can often be thought of as the result of two types of perturbations. Namely, there are physical forces imparted on suspended and attached particles by the aqueous phase. While suspended, particles can be accelerated towards the surface of the coal matrix leading to capture of the particle or detachment of additional fines. Whereas, for attached particles, the fluid imparts both drag and lift which act to mobilise

the colloid into the solution. Additionally, the physicochemical interactions that take place during colloid-colloid and colloid-surface perturbations can have a strong impact on particle behaviour (Ryan and Elimelech, 1995). This involves attractive and repulsive electrostatic forces between solid interfaces. In this investigation, these forces are taken according to Derjaguin-Landan-Verwey-Overbeek (DLVO) theory, which summarises colloidal interactions as the superposition of London-van der Waals and electric double layer (EDL) energies.

*2.1.1. DLVO Theory*

The expressions for drag, lift and gravity forces on a solid spherical particle in a fluid are quite common in the literature. It is when investigating the electrostatic interactions between particles that are separated by distances on the order of nanometres that a complete understanding is lacking (Liang et al., 2007). Classical DLVO theory takes the assumption that interaction forces between solid surfaces in a liquid can be taken as a superposition of London-van der Waals attraction energy and the double layer electric effect (Liang et al., 2007).

Since first proposed in the 1940s, DLVO theory has been subject to considerable experimental testing, showing both strengths and weaknesses (Daintith, 2008). A primary weaknesses is that of describing colloidal behaviour in an aggregated state, at which short-range interactions (surface separations of the order of 1 $nm$) such as the Born potential become important due to the specific properties of ions. When formulating a DEM simulation for the detachment scenario, these interactions are neglected due to the time-scale requirements needed to capture stable behaviour at this resolution. As a result, a *cut-off* distance on the order of $10^{-8}$ $m$ or 1% of particle radii is defined in line with a smooth geometry assumption. Using this cut-off distance tends to create a primary energy minimum at the point of particle contact causing captured particles to have no surface separation distance.

*2.1.2. London-van der Waals Attraction*

It was noted by Hamaker (1937) that the apparent adhesion forces between small particles of any substance or a particle and a surface was a common occurrence in colloidal systems with processes such as flocculation being the most striking example. The attractive force originates due to dipoles of atoms interacting between colloids over finite distances. This relatively weak interaction energy becomes significant when integrated over solid bodies at

the microscale and can dominate their behaviour. The works of Bedrikovetsky et al. (2011) and Khilar and Fogler (1998) perform this integration using the comparison of a sphere to a flat plate under the philosophy that, relative to a colloid, the surface is similar to a particle with infinite radius. Under this assumption, the London-van der Waals energy potential is given by Equation 1[1] and is a function of the ratio of the minimum surface separation to the diameter of the particles, $x$. The other parameters of importance include the ratio of interacting particle diameters, $y$, and the Hamaker constant, $A_{132}$, which are determined by the system environment.

$$V_{LvdW} = -A_{132}\frac{1}{12}\left(\frac{y}{x^2+xy+x} + \frac{y}{x^2+xy+x+y} + 2ln\frac{x^2+xy+x}{x^2+xy+x+y}\right) \tag{1}$$

In order to formulate a flat plate to sphere relation, the value of $y$ is taken to infinity (Hamaker, 1937), giving,

$$V_{LvdW} = -A_{132}\frac{1}{12}\left(\frac{1}{x} + \frac{1}{x+1} + 2ln\frac{x}{x+1}\right), \quad y \to \infty. \tag{2}$$

If one then takes $Z = \frac{x}{2}$, equivalently the ratio of surface separation to particle radius one obtains the expression used by Bedrikovetsky et al. (2011),

$$V_{LvdW} = \frac{-A_{132}}{6}\left[\frac{2(1+Z)}{Z(2+Z)} + ln\left(\frac{Z}{2+Z}\right)\right]. \tag{3}$$

When formulating the problem with the DEM, inter-particle reactions are of key interest. As such, rather than taking the sphere-flat plate simplification, it is necessary to capture the value of $y$. In order to do this, differentiation of Equation 1 with respect to surface separation is required to obtain the electrostatic attractive forces between colloids which gives,

$$F_{LvdW} = \frac{A_{132}}{12D_1}(2x+y+1)\left(\frac{y}{(X_1)^2} + \frac{y}{(X_2)^2} + \frac{2}{X_2} - \frac{2}{X_1}\right), \tag{4a}$$

in which,

$$X_1 = x^2 + xy + x, \tag{4b}$$

[1]Full details of surface integration to obtain energy terms can be found in Hamaker (1937)

and,

$$X_2 = x^2 + xy + x + y. \tag{4c}$$

Determining the value of the Hamaker constant is covered comprehensively in the literature. For a subsurface environment, the molecular properties of the fines ($A_{11}$), the porous surface ($A_{22}$) and the fluid ($A_{33}$) contribute to the value. For this, it is assumed that quartz is a reasonable approximation of the clay-like material and the resultant Hamaker constants for fines and the coal matrix are taken as,

$$A_{11} \approx A_{22}. \tag{5}$$

The production fluid extracted from a CSG reservoir is generally termed brine, which is simply salty water for which the Hamaker constant can be seen in Table 1.

Table 1: Hamaker constants used for major components of the subsurface environment.

| Nomenclature | Component | Approx. Material | Hamaker Constant $[J]$ |
|---|---|---|---|
| $A_{11}$ | Fines | Quartz ($SiO_2$) | $6 \times 10^{-20}$ |
| $A_{22}$ | Coal matrix | Quartz ($SiO_2$) | $6 \times 10^{-20}$ |
| $A_{33}$ | Production fluid | Water | $4 \times 10^{-20}$ |

Equation 6 is then applied in order to find the overall Hamaker constant for the system (Khilar and Fogler, 1998).

$$A_{132} \approx (A_{11}^{0.5} - A_{33}^{0.5})(A_{22}^{0.5} - A_{33}^{0.5}) = 2.02 \times 10^{-21} J \tag{6}$$

*2.1.3. Electric Double Layer Repulsion*

A principle characteristic of colloidal particles is their surface charge as a result of ion exchange with the surrounding fluid. The region over which this affects the fluid solution is termed the electric double layer (EDL). When the EDL of two like-charged particles overlap a repulsive force is generated. The effect of a negatively charged surface attracts positively charged ions in a tight layer to the bounding surface known as the Stern layer. As one moves further from this layer, there is an exponential decay in the electrokinetic potential as ions diffuse and eventually become unaffected in the bulk solution.

The region about a solid surface can generally be broken up into three sections, namely the Stern layer, diffuse layer and the bulk solution. The Stern layer accounts for the finite size of ions limiting their proximity to the surface. As such, this specifies the proximity with which they can approach the solid surface and over which only linear decay in the electrostatic potential is expected. Introduced in the Stern model in the 1920's, the formulation of this layer built on the Gouy-Chapman model which assumed exponential decay from the solid boundary. For the purposes of this investigation, it is appropriate to neglect the Stern layer due to distance cut-off's implemented in the simulation scheme, however, the exponential decay described by the Stern model outside of this region remains valid.

There are a variety of formulations of the EDL interaction energy between solid bodies in solution dependent on geometries and the EDL model utilised (i.e. Stern, Guoy-Chapman, Helmholtz etc.). Fines migration models described in Bedrikovetsky et al. (2011) and Khilar and Fogler (1998) use the formulation shown in Equation 7 with nomenclature described in Table 2.

$$V_{EDL} = \frac{\varepsilon_0 D_e r_s}{4}\left[2\psi_{01}\psi_{02} ln\left(\frac{1+exp(-\kappa h)}{1-exp(-\kappa h)}\right) - (\psi_{01}^2+\psi_{02}^2) ln(1-exp(-2\kappa h)\right] \tag{7a}$$

$$\kappa = 0.73\times 10^8 \sqrt{\sum C_{mi} z_i^2} \tag{7b}$$

Table 2: Summary of DLVO interaction parameters

| Nomenclature | Parameter | Units |
|---|---|---|
| $C_m$ | Fluid phase salinity | $mol/m^3$ |
| $D_e$ | Dielectric constant | $-$ |
| $h$ | Solid phase separation distance | $m$ |
| $r_s$ | Particle radius | $m$ |
| $z_i$ | Electrolyte valence | $-$ |
| $\varepsilon$ | Electric constant (permittivity of free space) | $C^{-2}J^{-1}m^{-1}$ |
| $\kappa$ | Inverse Debye length | $-$ |
| $\psi$ | Surface potentials | $V$ |

A comparative formulation was presented in the work of Zhang and Zhang (2011) in which the LBM was employed to investigate particle agglomeration, and this is seen in Equation 8. Similar to the London-van der Waals

interaction, in a DEM simulation the preferential formulation of interaction energies is sphere-to-sphere allowing the influence of the migrating fines on those attached to be evaluated. Additionally, the resultant force on varying sized particles must also be captured as a distribution of radii can be expected in the subsurface environment. As a result of this, the EDL model described by Zhang and Zhang (2011) was incorporated into the numerical model developed here. This is based on Stern theory where the interaction force between two particles $i$ and $j$ is given as,

$$F_{EDL} = \frac{4\pi\varepsilon_a \kappa r_i r_j \psi^2}{r_i + r_j} exp(-\kappa h). \tag{8}$$

These electrostatic interactions play a key role in the behaviour of fines detachment and capture kinetics. The small-scale model approach to fines liberation in this paper provides an insight into the behavioural results these forces have on particles. This enables further understanding of the detachment process as well as potential support to continuum models.

### *2.2. Detachment Kinetics*

Determining the mechanical equilibrium of an attached particle is a widely recognised and utilised method of determining colloid detachment. This is approached through either a balance of torques, or investigating the balance of drag and friction using an empirical Coulomb coefficient. The two approaches are mathematically equivalent (Bedrikovetsky et al., 2011). The torque balance approach will be presented here as the formulation of electrostatic forcing terms are applicable to the DEM modelling discussed in Section 3.1. However, in using DEM the need for explicitly balancing torques is unnecessary as direct simulation of interacting forces is conducted.

Considering the case of a particle attached to the lower surface of a face cleat, one is able to conceptualise the forces present. The fluid flow can be expected to generate drag and lift, while electrostatic and gravitational forces will act to retain the particle, as shown in Figure 1. This configuration is in line with the work of Bedrikovetsky et al. (2011). It should be noted that gravity will not always be retentive, for example on the upper surface of a face cleat or in a butt cleat. However, although gravity has an effect on the stability of migrating particles its effect is not significant when particles are electrostatically attached.

The forces acting on the topmost particle are given in recent papers by Al-Abduwani et al. (2005) and Bedrikovetsky et al. (2011) using Hele-Shaw flow

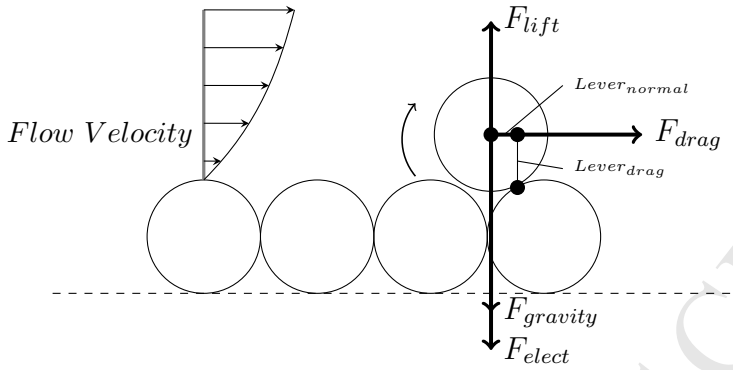


Figure 1: Diagramatic view of the forces acting on a particle during detachment (recreated from Bedrikovetsky et al. (2011)).

relations[2]. Equations 9 and 10 indicate that the detaching lift and drag forces both increase with fluid velocity, while attachment forces are independent of the flow.

$$F_{drag} = \frac{\omega \pi \mu r_s^2 v}{H} \qquad F_{lift} = \chi r_s^3 \sqrt{\frac{\rho \mu v^3}{H^3}} \tag{9}$$

$$F_{gravity} = \frac{4}{3}\pi r_s^3 \Delta\rho.g \qquad F_{elect} = -\frac{\partial V}{\partial h} \tag{10}$$

The additional parameters used in detachment and attachment Equations 9 and 10 are presented in Table 3 along with dimensions.

The forces presented were stated in the literature, but it can be seen that empirical correlations are still required in the drag and lift calculations. During this investigation the hydrodynamic forces are computed directly from the immersed moving boundary technique used to couple the LBM and DEM, as discussed in Section 3.3. Physicochemical colloidal interactions are incorporated via an explicit implementation of the phenomenological models into the DEM framework.

Directly calculating the interactions on the grain-scale enables the analysis of approximated forcing terms used in advection-dispersion models. The

[2] *Hele-Shaw Flow* - fluid flow between parallel plates separated by a small distance, $H$.

[3] $V$ - Energy potential as described by DLVO theory, and equal to the sum of van der Waals, Born and double electric energies. See Bedrikovetsky et al. (2011) for further details.

Table 3: Summary of detachment and attachment force parameters.

| Nomenclature | Parameter | Units |
|---|---|---|
| $\omega$ | Empirical correction constant | - |
| $\mu$ | Fluid viscosity | $Pa.s$ |
| $v$ | Interstitial flow velocity | $m/s$ |
| $r_s$ | Particle radius | $m$ |
| $H$ | Channel width - (CSG pore opening size) | $m$ |
| $\chi$ | Lifting correction constant | - |
| $\rho$ | Fluid density | $kg/m^3$ |
| $\Delta\rho$ | Difference in particle and fluid density | $kg/m^3$ |
| $g$ | Acceleration due to gravity | $m/s^2$ |
| $V$ | Energy potential[3] | $J$ |

first investigation undertaken in this report looks at the dislodgement number used in the works of Bedrikovetsky et al. (2011) as a tuning parameter to assess the quantity of fine particles in solution.

## 3. Direct Numerical Simulation of Colloidal Fines

The modelling of particle suspensions is a non-trivial task for traditional, grid-based fluid dynamics solvers. In this work, the lattice Boltzmann method (McNamara and Zanetti, 1988; Chen and Doolen, 1998) has been employed as an alternative approach to simulate fluid flow. This technique was then coupled with the discrete element method (Cundall and Strack, 1979), which is a Lagrangian model used to predict the trajectories of solid particles undergoing Newtonian motion. Hydrodynamic coupling of the two methods via an immersed moving boundary condition (Noble and Torczynski, 1998; Cook et al., 2004) facilitated the modelling of particle suspensions at solid volume fractions up to the theoretical packing limit. This LBM-DEM framework captures detailed particle-particle, particle-boundary, and particle-fluid interactions and has been successfully applied in a number of erosion (Cook et al., 2004; Lomin et al., 2013) and fines transport problems (Leonardi et al., 2012a,b).

### *3.1. The Discrete Element Method*

The DEM is an explicit numerical method that can be used to simulate an assemblage of distinct particles, discretise a granular continuum, or do both

at the same time. In this method the translation and rotation of particles are governed by Newton's Second Law for forces,

$$m_i \mathbf{a_i} + c_t \mathbf{v_i} = \sum_j \mathbf{F_{ij}}, \tag{11}$$

and torques,

$$I_i \boldsymbol{\alpha_i} + c_r \boldsymbol{\omega_i} = \sum_j \mathbf{T_{ij}}, \tag{12}$$

in which $c_t$ and $c_r$ are damping coefficients, and the terms associated with them represent viscous forces to account for the effect of dissipation in a system (Cundall and Strack, 1979). For fines in a coal seam the total forces and torques are comprised of hydrodynamic ($F_{hydro}$), electrostatic ($F_{elec}$), gravitational ($F_{grav}$), and mechanical ($F_{contact}$) components. In addition, lubrication forces are present with particles approaching and separating from contact. To capture this, a phenomenological model is applied in the DEM framework and is described in Section 4.2.1.

The mechanical forces in the DEM arise from particle-particle and particle-boundary interactions which are typically resolved using a soft-contact model. This class of contact, as shown schematically in Figure 2, permits a small amount of overlap between contacting bodies which is used in the calculation of repulsive normal and tangential forces. A range of relations for normal contact forces are available including Hertzian, Winkler and Power Law (Han et al., 2000a). However, a linear Hooke model is employed in this study for particle contact force,

$$F_{contact} = \begin{cases} 0 & if \quad \delta \leq 0 \\ k_n \delta & if \quad \delta > 0 \end{cases} \tag{13}$$

in which $\delta$ is the overlap between the particle boundaries and $k_n$ is the normal stiffness, or penalty, which can be related to the elastic modulus of the material. The tangential force component is calculated similarly using relative tangential displacement instead of normal overlap and incorporating Coulomb friction (Han et al., 2000b).

Resolving contact forces in the DEM first requires the identification of pairs of potentially contacting bodies and this becomes non-trivial when a large number of particles is present in the simulation. Naively assessing the

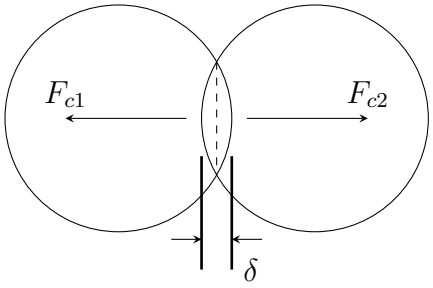


Figure 2: Contact modelling of an idealised two-particle interaction in the DEM.

contact of $N$ particles with all other bodies in the domain would produce a search problem of $O(N^2)$, with each particle having $N-1$ possible objects to contact with. Williams and O'Connor (1999) showed that with a test of 1000 two-dimensional objects, over 90% of computational time is spent in the contact detection stage if special considerations are not taken. In this work a *no binary search* (NBS) algorithm is used to reduce the overhead associated with contact detection however a number of different tree and cell-based algorithms are available (Williams and O'Connor, 1999).

The position, velocity and acceleration of DEM particles are updated using an explicit time integration scheme. This scheme, and the associated time step, must be chosen carefully so as to maintain simulation accuracy and stability. Here, a velocity Verlet integration scheme is utilised in conjunction with a Courant-Friedrichs-Lewy condition,

$$\Delta t_{DEM} \leq \lambda \sqrt{|\frac{m}{k_n}|_{min}}, \tag{14}$$

which governs the size of the DEM time step. Here, $\lambda$ is a constant (typically $\sim 0.1$) and $|m/k_n|_{min}$ represents the minimum combination of mass, $m$, and normal contact stiffness for all particles. The sequence of contact search, contact resolution, force summation, and kinematic integration is then executed at each time step until the simulation has reached its conclusion.

### *3.2. The Lattice Boltzmann Method*

Over the past three decades the LBM has been established as a powerful alternative to conventional computational fluid dynamics. Its use has been well documented in both research and commercial settings with a variety of applications in fluid mechanics including porous media flows, vehicle aerodynamics, multiphase and multicomponent flows, and particle suspensions.

In the LBM, fluid behaviour is simulated at the mesoscopic scale rather than the macroscopic scale with the latter typically involving the discretisation and integration of the Navier-Stokes equations. Instead, the fluid domain is discretised into packets of mass termed particle distribution functions (PDFs), $f_i$, which represent the probability that a molecule with velocity $\mathbf{c}_i$ can be found at position $\mathbf{x}$ and time $t$. These PDFs reside on a lattice, or grid, and are evolved via the lattice Boltzmann equation according to relationships that conserve both mass and momentum. In this study the linearised Bhatnagar-Gross-Krook (BGK) (Bhatnagar et al., 1954) form of the lattice Boltzmann equation is employed. This is described in lattice units as,

$$\overbrace{f_i(\mathbf{x}+\mathbf{c}_i, t+1) = f_i(\mathbf{x}, t)}^{streaming} \underbrace{-\frac{1}{\tau}(f_i(\mathbf{x}, t) - f_i^{eq}(\mathbf{x}, t))}_{collision(\Omega_i^{BGK})}, \tag{15}$$

in which $f_i^{eq}$ represents the Maxwellian equilibrium distribution function of $f_i$ and $\tau$ is the monotonic relaxation parameter of the collision operator, $\Omega_i^{BGK}$.

Inspection of Equation 15 shows that the LBM is generally broken into two steps defined as streaming and collision. The order in which these steps are performed is irrelevant, but the purpose of each step is important. During streaming the PDFs, $f_i$, located at $\mathbf{x}$ are moved to the lattice node located at $\mathbf{x} + \mathbf{c}_i$. The collision step then redistributes PDFs at a lattice node as a consequence of interaction with the other incoming distribution functions.

The calculation of macroscopic fluid variables in the LBM is straightforward. The nodal density,

$$\rho = \sum_i f_i, \tag{16}$$

and momentum flux,

$$\rho\mathbf{u} = \sum_i f_i \mathbf{c}_i, \tag{17}$$

are both defined as local moments of the PDFs, with $\mathbf{u}$ the macroscopic fluid velocity.

The family of lattices available for use in the LBM can be generally described as D$i$Q$j$ where $i$ is the dimension of the problem and $j$ is the number

of velocities in the lattice. For example, the D2Q9 lattice which is commonly used in two-dimensional models is based on an orthogonal arrangement and features a rest velocity, four nearest-neighbour velocities, and four next-nearest-neighbour velocities. In this study a D3Q15 lattice is employed and this is shown schematically in Figure 3.

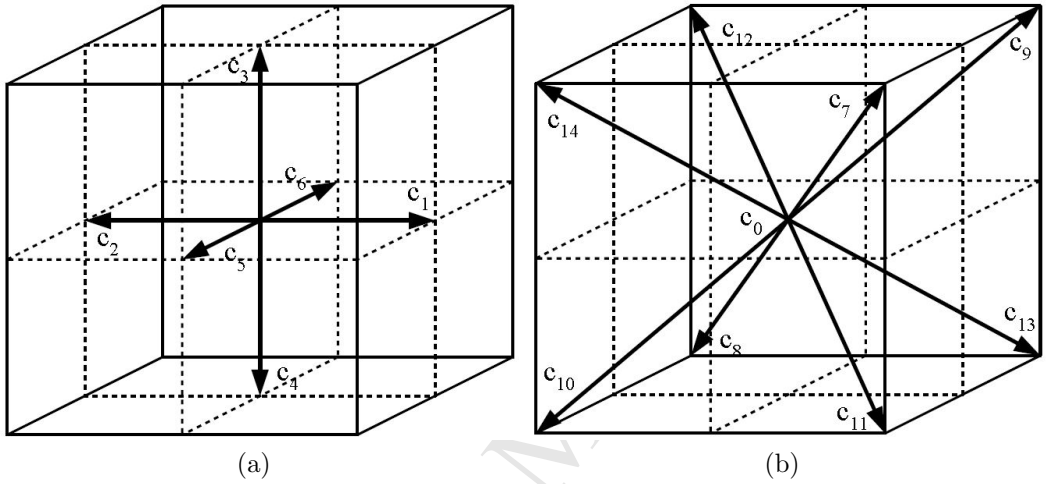


Figure 3: The (a) orthogonal and (b) bidiagonal velocity discretisation of the D3Q15 lattice in the LBM.

It has been widely shown in the literature that the correct implementation of the lattice Boltzmann method is able to recover the Navier-Stokes equations in the near-incompressible limit to second order accuracy for both temporal and spatial parameters (Chen and Doolen, 1998). This is done through a multiscale Chapman-Enskog expansion that consists of first expanding the lattice Boltzmann equation about a smallness parameter, $\delta$, before conducting a two-time expansion to track the transport interactions on a diffusive and convective scale. In general when performing this form of analysis, one aims to take natural selections of expansion parameters to ensure a useful solution is obtained. In practice $\delta$ is taken as the Knudsen number[4] while the short-time scale $t_0$ is chosen in order to describe convective behaviours while $t_1$ is used for diffusive behaviours that occur on a long time

[4] *Knudsen number:* ratio of the molecular mean free path to a representative physical length scale

scale. The Chapman-Enskog analysis results in the complete description of the equilibrium distribution functions, $f_i^{eq}$, and permits the definition of an equation of state for the fluid pressure,

$$p = \frac{c^2 \rho}{3}, \tag{18}$$

in which $c = \Delta x / \Delta t_{LBM}$ is termed the lattice speed. It also results in the definition of the kinematic fluid viscosity, $\nu$, as a function of the lattice spacing, time step and relaxation parameter,

$$\nu = \frac{1}{3}\left(\tau - \frac{1}{2}\right)\frac{(\Delta x)^2}{\Delta t_{LBM}}. \tag{19}$$

Consideration of Equation 19 highlights the interdependence of the time step, lattice spacing, fluid viscosity and relaxation parameter. In defining a LBM simulation it is common practice to prescribe the desired viscosity along with a lattice spacing that discretises the domain at sufficient resolution. The relaxation parameter can then be used as a free parameter in the calculation of the LBM timestep. However, Equation 19 shows that $\tau > 1/2$ is required to maintain positive viscosity. In addition, as $\tau \to 1/2$ the stability of the BGK-LBE decreases (Sterling and Chen, 1996) while as $\tau$ increases the accuracy of the LBM simulation may decrease as a consequence of the chosen hydrodynamic boundary conditions (Pan et al., 2006).

### *3.3. Hydrodynamic Coupling of Solid and Fluid Phases*

The LBM has been shown to be capable of modelling fluid flows in accordance with the Navier-Stokes equations while the DEM utilises Newtonian physics to predict particle behaviour. A range of boundary conditions, both *immersed* and *dry*, are then available for the hydrodynamic coupling of the two methods. A selection of these techniques is discussed briefly as follows.

The bounce-back method is typically used to implement no-slip conditions on stationary boundaries and as such it can be used in the case of impermeable walls. In this study, it is utilised to simulate the hydrodynamic constraints of the coal about a face or butt cleat. The benefits of using this boundary condition are those of simplicity, locality, and relative accuracy for the desired scenario. There exists two common variants of this method, namely *on-grid* and *mid-grid*. Succi (2001) and many others have reported that the on-grid method is only first-order accurate, while a mid-grid approach maintains the second-order accuracy of the LBM.

The link bounce-back (LBB) method was proposed by Ladd (1994a,b) as an improvement to the bounce-back technique for modelling fluid-particle interaction with moving boundaries. This is an immersed technique, meaning that moving obstacles are mapped to the underlying LBM lattice so that fluid is present in the space inside the obstacle. As the name suggests, the LBB method enforces the bounce-back condition on the links between fluid boundary nodes and solid boundary nodes and assumes that the solid-fluid interface exists in the middle of each link. (i.e. halfway between the fluid boundary nodes and solid boundary nodes). The covered LBM nodes are relaxed towards the the rigid body velocity of the obstacle at the corresponding location, with the associated change in fluid momentum transferred to the obstacle. Over the past two decades, this popular coupling method has evolved to address fluctuations in the hydrodynamic drag and torque (Verberg and Ladd, 2000, 2001) as particles move across the underlying lattice, as well as issues related to the *actual* location of the no-slip boundary during simulations (Chun and Ladd, 2007).

In contrast to the LBB and its derivatives, Aidun et al. (2000) proposed an approach in which fluid is not permitted to exist within solid obstacles, meaning that no inertial force is applied to the obstacle from the internal fluid (a well-known artefact of immersed techniques). This facilitates the modelling of obstacles with a solid density close to or less than the fluid density. In this dry coupling method, the fluid-obstacle boundary links, the boundary velocity, and the bounce-back of PDFs are determined as in the LBB. As an obstacle traverses the lattice, LBM nodes are simultaneously covered and uncovered requiring the destruction and creation of PDFs, respectively. The total force on the obstacle is found by the summation of forces over all fluid boundary nodes, newly covered nodes, and newly uncovered fluid nodes. As in the LBB, the discontinuity of force with time can be an issue. Also, the creation and destruction of fluid mass means that this technique is not locally mass conservative (although it should conserve mass globally) and that it can be computationally inconvenient to implement.

In this work, the immersed moving boundary (IMB) condition (Noble and Torczynski, 1998) is used to calculate the hydrodynamic forces and torques acting on particles. This couples the movement of fines particles to the macroscopic fluid behaviour and vice versa. The partial bounce-back approach of the IMB results in computations that are completely local, which is convenient. When appropriately formulated, the IMB has been shown to approach second-order grid convergence, and its potential has been demonstrated in

similar investigations by Cook et al. (2004) and Lomin et al. (2013), which model particle suspensions and in certain cases look at erosional issues. In order to do this, a weighting function was developed that assesses the fraction of a node that is solid and liquid, as well as an additional collision term to account for solid obstacle interactions. Incorporating these, Equation 15 evolves to,

$$\overbrace{f_i(\mathbf{x}+\mathbf{c}_i, t+1) = f_i(\mathbf{x},t)}^{streaming} \underbrace{-\frac{1}{\tau}(1-B_n)(f_i(\mathbf{x},t) - f_i^{eq}(\mathbf{x},t)) + B_n\Omega_i^s}_{modified \quad collision}, \tag{20}$$

in which $B_n$ approaches unity for high solid fraction cells and zero in bulk solution.

The additional collision term ($\Omega_i^s$) has been defined in multiple ways in the literature. The first method is based on the bounce-back of the non-equilibrium part of the particle distribution function and the second by superimposing the equilibrium distribution function of the particle velocity and a term dependent on the deviation of the current distribution from its equilibrium value.

One of the primary benefits of the IMB is that it allows the momentum transferred between phases to be quantified. It is more convenient to perform this calculation in lattice units in which the hydrodynamic force on a particle, $j$, is given by the summation of momentum changes in the particle distribution functions,

$$F_j = \sum_n B_n \left( \sum_i \Omega_i^s c_i \right). \tag{21}$$

When considering a particle, $j$, it is evident that the fluid velocity will not be constant at each solid boundary node. Due to this, a hydrodynamic torque is also imposed,

$$T_j = \sum_n \left[ (x_n - X_j) \times B_n \left( \sum_i \Omega_i^s c_i \right) \right]. \tag{22}$$

The hydrodynamic interactions are then used as inputs into the DEM model allowing the coupling of fluid and solid phases to be complete.

The LBM-DEM approach coupled via the IMB technique provides the relevant theoretical basis for the developed small scale model investigating fines detachment and transport in coal seams. The framework created, along with the investigative processes conducted, act to increase the understanding of fines migration and provide capability for further analysis.

### *3.4. Lubrication Effects*

It is widely accepted (Aidun and Clausen, 2010) that when two moving particles in suspension approach contact, the associated hydrodynamic forces are not correctly predicted by the LBM. As the separation between the boundaries decreases, the number of lattice nodes available to resolve the flow approaches zero. This means that the pressure singularity which can occur in such scenarios is not captured. It should be noted, however, that the significance of these lubrication effects depend on the particle Reynolds number and the relative size of surface asperities.

In an attempt to address the lubrication issues in LBM simulations of suspensions, Ding and Aidun (2003) used local grid spacing adjustments with limited success. For two spherical particles, Kim and Karrila (1991) defined phenomenological expressions for three modes of contact lubrication forces, namely normal, tangential and rotational. Nguyen and Ladd (2002) incorporated these forces in LBM simulations of fluid-particle systems using an implicit solution strategy. A similar approach is taken in this work, however only the normal force is considered and this is incorporated as an additional term in the DEM framework and solved explicitly. The lubrication force between particles is given as a function of the surface separation, $h$, the particle velocities, $\mathbf{u}_i$, and the unit vector between the particles, $R_{12}$. Additionally, it relies on the particle radii, $a_1$ and $a_2$, the fluid viscosity, $\mu$, and the cut off distance, $h_N$, which are treated as constants through simulations,

$$\mathbf{F}_{lub} = -6\pi\mu \left( \frac{a_1 a_2}{(a_1 + a_2)} \right)^2 \left( \frac{1}{h} - \frac{1}{h_N} \right) (\mathbf{u}_1 - \mathbf{u}_2) \cdot \mathbf{R}_{12}. \tag{23}$$

It is noted that this force tends to infinity as the surface separation approaches zero, and as such a cut-off distance was set at 1% of the particle radii, which is in alignment with the DLVO implementation. Given the size of the particles considered in this study, this cut-off distance is appropriate

when the presence of surface asperities on the order of nanometers is considered. For a more in depth discussion of lubrication forces and particles near contact, the reader is referred to Chapter 9 of Kim and Karrila (1991).

### *3.5. Implementation of Colloidal Forces*

A number of theoretical relations have been identified to simulate the behaviour of fines inside a porous coal matrix. In DLVO theory and the LBM-DEM framework there are a number of inherent assumptions that need to be incorporated in the modelling philosophy to ensure numerical stability. The first relates to the geometry of particles to be modelled. Fines are considered as smooth spheres while the coal matrix surface is approximated by fixed spheres to account for a small degree of surface irregularity. Fixing a layer of spheres as a bounding surface gives an approximation of a deep particle layer without the additional computational costs. In line with neglecting surface irregularities, a cut-off separation distance was implemented within which electrostatic forces are assumed constant. This assists with numerical contact stability and allows for a reasonable time-step to be used in iteration.

In terms of the electrostatic interactions, non-DLVO forces are not considered to be significant in the system. This includes energies of the form of *Born repulsion* and *AB (acid-base) interactions*. These act within the cut-off distance where assumptions of smooth surfaced particles break down. Additionally, fines are modelled with a constant uniform surface charge. Note that the investigation of surface heterogeneities is widely studied and could be implemented into the framework at a later stage.

The aim of this study is specifically to assess the detachment behaviour of fines and to quantify the effect of physicochemical properties in relation to viscous stresses in fines migration. System parameters such as fluid (e.g. viscosity, density) and particle (e.g. stiffness, density) properties along with LBM-DEM solver parameters are held as constant as possible.

### *3.6. DEM-only Verification*

The computational implementation of DLVO forces was verified before undertaking more detailed simulations. Further validation of the model through Section 4 is completed by showing the ability to capture certain physical phenomena, this acts to provide evidence for the model to simulate more complex environments.

The preliminary testing of DLVO forces was performed inside a DEM-only domain with periodic conditions giving a $10 \times 10 \times 10 \mu m$ viewing window.

This test was used only to verify the calculation of DLVO forces for single and multi-particle interactions.

In order to further define the system under investigation, both the cohesive Bond ($Bo$) and Péclet ($Pe$) numbers are introduced. Here, the Bond number is defined as,

$$Bo = \frac{|F_{elect}|}{F_{gravity}}, \tag{24}$$

with the associated forces determined from simulation results which incorporated Equation 10. The results of two particles in contact can be seen in Figure 4b, where the maximum electrostatic force is found to be $8.08 \times 10^{-13}$ $N$. From this, and the calculation of gravitational forces, a cohesive Bond number of 1.49 is found. This indicates that cohesive forces are 149% that of gravity for a two particle contact, and this increases with the interaction of more bounding particles. Additionally, the Péclet number for a particle in channel flow is given as,

$$Pe = \frac{6\pi\mu\dot{\gamma}r_s^3}{k_B T}, \tag{25}$$

in which $k_B$ is the Boltzmann constant, $T$ is the absolute temperature and $\dot{\gamma}$ is taken as the maximum velocity divided by half of the flow channel height as per Semwogerere et al. (2007). For the LBM-DEM simulations in Section 4, the lowest applied pressure differential resulted in a maximum velocity through the flow channel of 17.3 $\mu m/s$. In this minimum case,

$$Pe = \frac{6\pi \times 10^{-3} \times 17.3 \times 10^{-6} \times (2 \times 10^{-6})^3}{1.38 \times 10^{-23} \times 293 \times \times 5 \times 10^{-6}} \approx 130, \tag{26}$$

which is of the order of the transition range of Brownian motion according to Semwogerere et al. (2007). However, this represents the lower bound for the single particle detachment tests, which range up to a flow velocity of 170 $\mu m/s$ and a corresponding Péclet number of $O(10^3)$. In larger scale migration tests, the Péclet number is $O(10^3 - 10^4)$ for which the effect of Brownian motion is negligible (Sane, 2005; Semwogerere et al., 2007).

*3.6.1. DLVO Verification Testing*

Initial verification of the DLVO implementation was tested using a two-particle, DEM-only (i.e. no fluid) scenario. Here, particles were placed within

close proximity such that DLVO interactions could be used to attract or repel the neighbouring particle. During these tests, electrostatic forces were captured over a range of surface separations and compared with results of Equation 4a for the London-van der Waals interaction, and Equation 8 for the electric double layer.

Figure 4a is indicative of particle capture where the particles approach until contact and capture. Although not physically correct as this neglects any frictional resistance from surrounding fluid, qualitatively this agrees with the DLVO equations as the attractive force tends towards infinity, increasing particle acceleration. It is seen in Figure 4b that quantitatively the electrostatic force captured by the model accurately follows the expected trend.

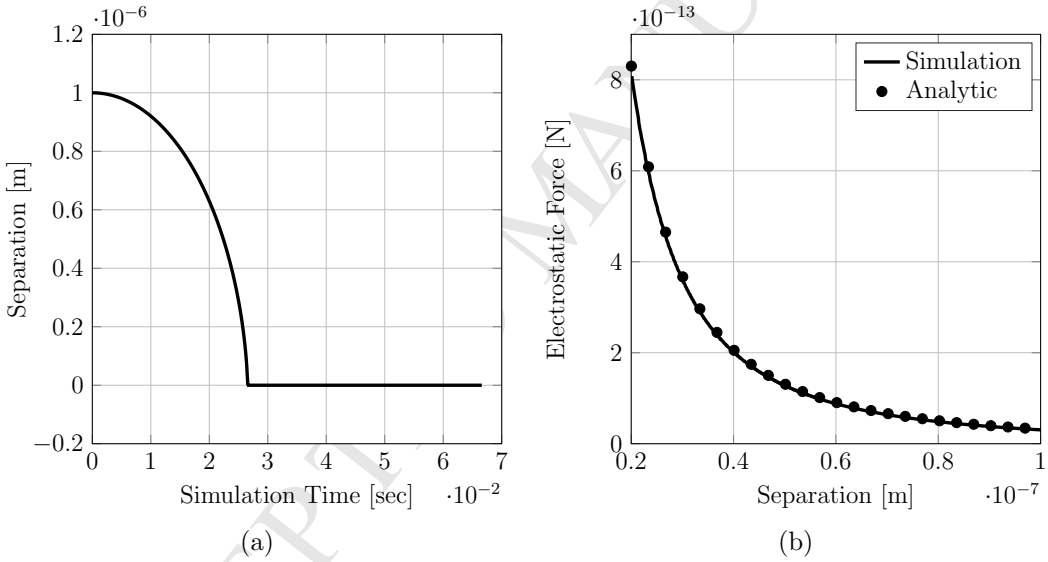


Figure 4: Results of the two-particle, DEM-only test used in the verification of the DLVO implementation showing the change in (a) separation with time and (b) electrostatic force with separation.

This test was then repeated for repulsive DLVO parameters for completeness prior to the implementation of multi-particle interactions. With the introduction of more particles, stable flocculation under attractive conditions and unstable dispersion when repulsive forces were dominant was observed. The structure of the initial states of these simulations can be seen in Figure 5, in which the particles have a radius of 2 $\mu m$ and density of $2650 kg/m^3$.

Figure 6a shows a comparison of the DLVO interaction force calculated

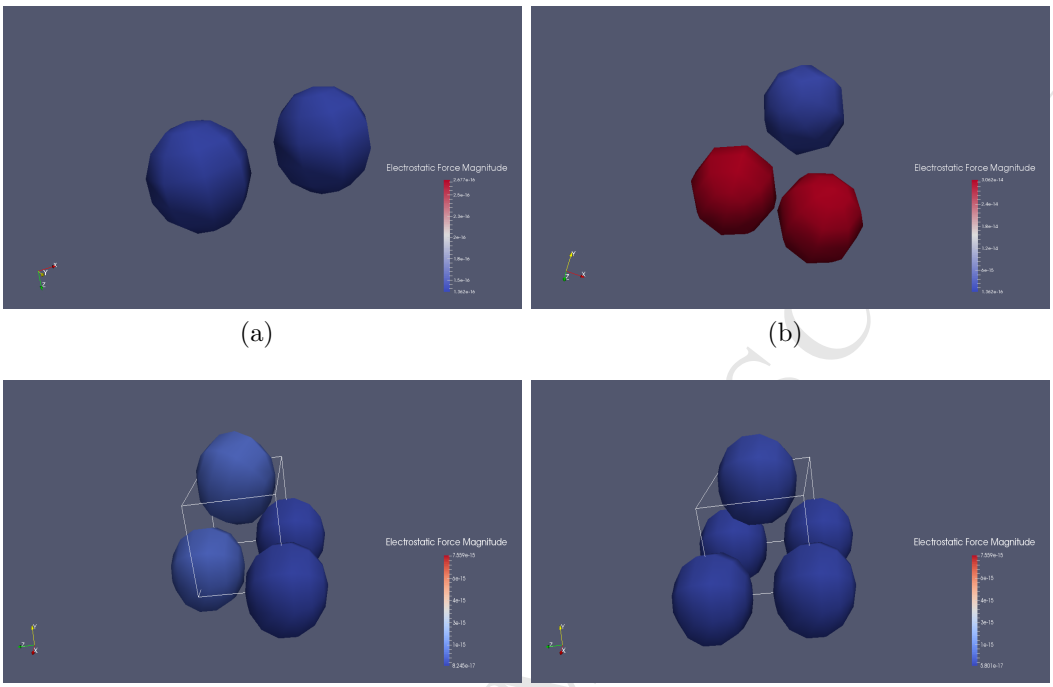


(a) (b)

(c) (d)

Figure 5: The arrangement of (a) two-particle, (b) three-particle, (c) four-particle, and (d) five-particle DEM-only simulations conducted in the verification of the DLVO implementation.

by simulation and that found analytically for a single particle in each initial state. It can be seen that the analytic and simulation results match prior to the force cut-off distance. Interesting to note is that the force calculated during the four-particle test appears to be capped at a lower value in comparison with the three-particle test. Further investigation into this saw that it was due to a slight rounding offset in the initial position of the free-to-move particle in the four particle simulation. This caused it to be captured by the single closest particle in the system, deeming the force of the two other particles negligible in the simulation time tested.

Figure 6b indicates that interaction energies for the five-particle test, although orders of magnitude less than other simulations, are present. This is seen by the gradually increasing particle velocity. The surface separation due to the position of the free-to-move particle is relatively large in comparison with lower dimensional tests. However, the results are still seen to match

with those analytically determined. This preliminary study verified that the implemented DLVO interaction law was working as expected in a DEM-only environment.

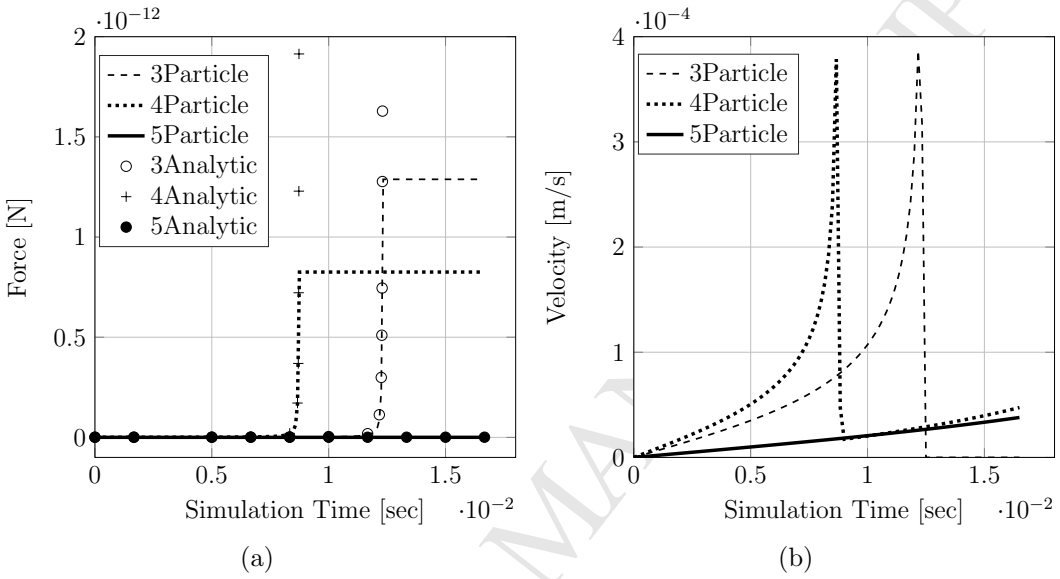


Figure 6: Results of the three, four and five-particle DEM-only tests used in the verification of the DLVO implementation showing (a) the total electrostatic force acting on and (b) the total velocity of the free-to-move particle.

### *3.6.2. Parametric Sensitivity*

A sensitivity analysis was performed to help elucidate the relationship between surface separation and DLVO forces for a range of parameters as summarised in Table 4. The results of this investigation are shown in Figure 7, including how the varying of certain parameters can shift the agglomeration process from stable to unstable. In these graphs the coordinate system implies that a negative and positive force is indicative of attraction and repulsion, respectively. It is evident that the Hamaker constant and Debye length have the largest impact on the particle behaviour. For this investigation, the Debye length was altered by reducing the salinity of the fluid in order to create repulsive electrostatic conditions.

Table 4: DLVO sensitivity testing parameters.

| Parameter | Nomenclature | Min Value | Max Value | Units |
|---|---|---|---|---|
| *London-van der Waals:* | | | | |
| Hamaker Constant | $A_{132}$ | $1 \times 10^{-22}$ | $1 \times 10^{-19}$ | $[J]$ |
| Diameter Ratio | $y$ | 0.5 | 5 | $[-]$ |
| *Electric Double Layer:* | | | | |
| Diameter Ratio | $y$ | 0.5 | 5 | $[-]$ |
| Debye Length | $k^{-1}$ | $1 \times 10^{-10}$ | $7.5 \times 10^{-9}$ | $[m]$ |
| Surface Potential | $\psi$ | $-10$ | $-50$ | $[mV]$ |

## 4. Investigation of Fines Liberation and Transport

The simulation parameters used in the following LBM-DEM tests were held constant across all scenarios. Fluid properties were specified to represent water at approximately 20 $^oC$ (density of 1000 $kg/m^3$ and viscosity $1 \times 10^{-6}$ $m^2/s$). The grid spacing for test cases was 0.5 $\mu m$ and the time step was chosen such that the lattice relaxation parameter was equal to one based on Equation 19. The result of this was a time step of $4.17 \times 10^{-8}$ $s$. Unless otherwise stated the particle diameter of 4 $\mu m$ was used giving eight grid spacings across each particle. It is also noted here that the specified time step above is implemented in both the LBM and DEM schemes and as such no sub-cycling of the either is required.

### *4.1. Examination of Dislodgement Number*

Following the verification of the DLVO contact law, the first study undertaken investigated LBM-DEM grid independence and in doing so explored one of the facets that appeared to be lacking depth in the particle detachment literature. The formulation of a maximum retention function by Bedrikovetsky et al. (2011) made a number of assumptions in the prediction of detachment kinetics. This was done by taking a torque balance about a point considered as a pin-joint. From here, the balance of normal forces (electrostatic, gravitational and lift) are compared with drag. In this, the electrostatic force is assumed to have a vertical force contribution only and approximations as to the length of lever arms in each respective direction are made. Additionally, empirical values are required to compute the hydrostatic drag and lift forces as seen in Equation 9, this introduces the need for historical data to

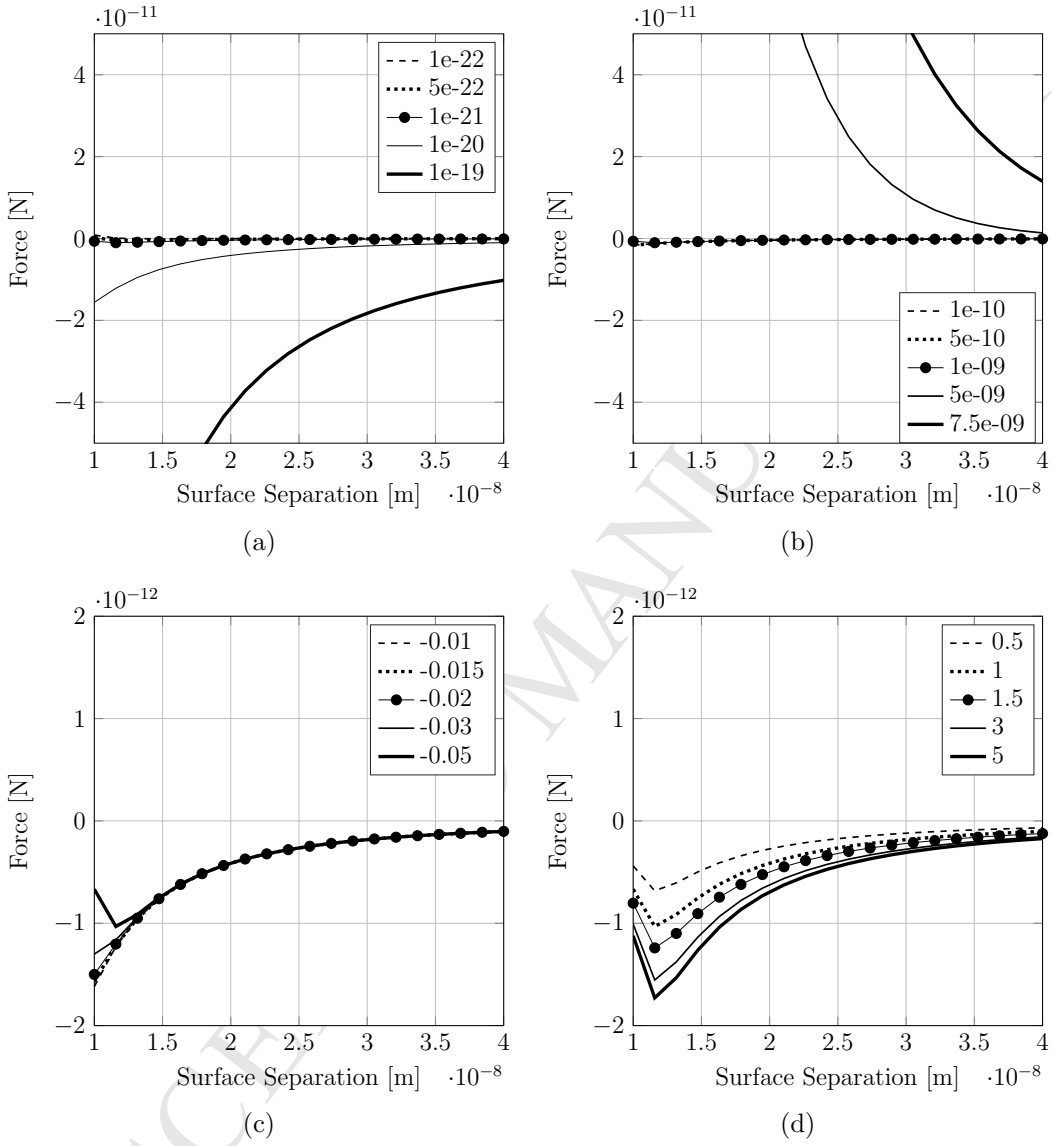


Figure 7: Results of the sensitivity testing of DLVO parameters used to explore the creation of repulsive and attractive environments, highlighting the effect of varying (a) the system Hamaker constant, (b) the Debye length, (c) the zeta potential, and (d) the particle interaction size ratio.

tune the resultant advection-diffusion (AD) model (see Bedrikovetsky et al. (2011) for an in-depth analysis of the AD model).

The maximum retained concentration of fines is described as a function of the dislodgement number which is proportional to the ratio of drag to normal forces and is given by Bedrikovetsky et al. (2011) as,

$$\varepsilon = \frac{\mu r_s^2 u}{H F_N}, \tag{27}$$

where $\mu$ is the dynamic viscosity of the fluid and $F_N$ is the sum of forces acting in the vertical direction as found from Hele-Shaw flow relations and DLVO theory and the maximum expected electrostatic force (Equations 9 and 10). The purpose of this dimensionless parameter is to assess if detachment is expected under various flow and electrostatic conditions.

In order to test the accuracy of this formulation, a test domain was constructed to replicate the detachment procedure shown in Figure 8. The geometry of the domain is $30 \times 10 \times 7$ $\mu m$ with periodicity in the x- and z-directions while wall boundaries are implemented using the bounce-back method. The fluid is driven by an applied body force, as is common practice in LBM simulations. The fluid properties were chosen to match that of water with a density of 1000 $kg/m^3$ and a kinematic viscosity of $1 \times 10^{-6}$ $m^2/s$.

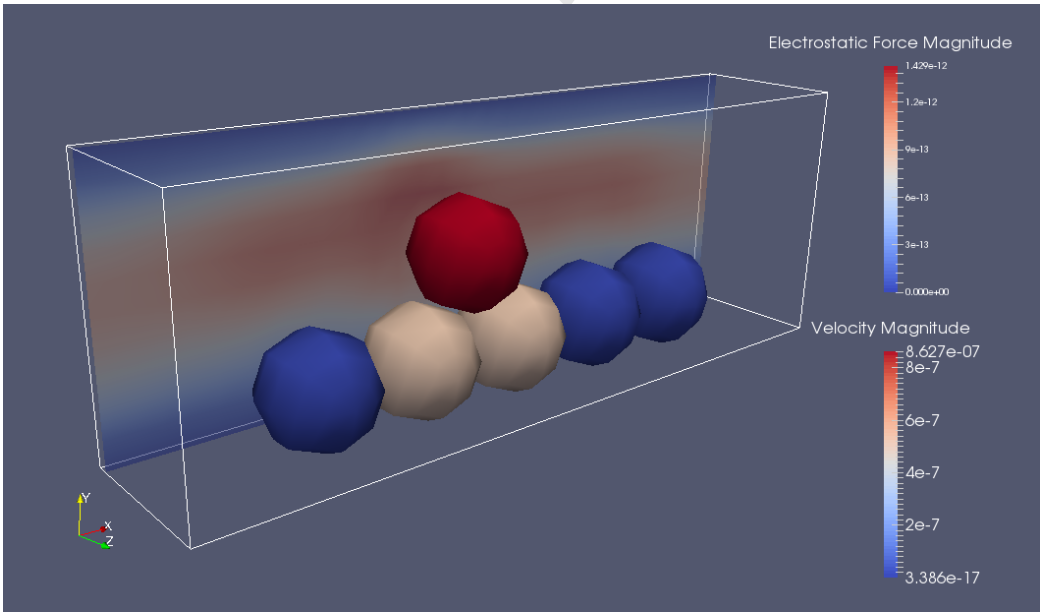


Figure 8: The layout of LBM-DEM simulations conducted for torque balance assessment in the investigation of dislodgement number.

Measuring the forces acting on the top layer particle enabled the dislodging number to be calculated under varying flow velocities. Initially, the simulation was executed with the top-most particle unrestricted in its motion. The resultant forces determined at a simulation time of $8.33 \times 10^{-5}$ *sec* are shown in Figure 9, after this point particle motion was observed to clearly influence the hydrodynamic forces and relation to a dislodgement number becomes impractical.

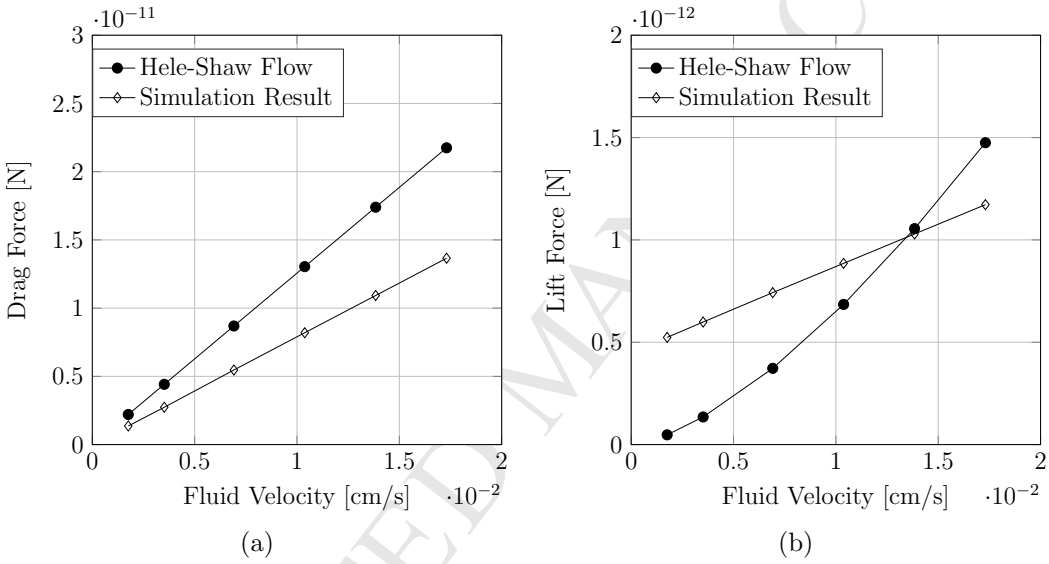


Figure 9: Results of initial torque balance testing used in the investigation of dislodgement number, including a comparison of the simulation (a) drag ($\omega = 60$) and (b) lift ($\chi = 1190$) to the respective Hele-Shaw results.

Figure 9 indicates quite a substantial difference between empirically predicted results and those found in the simulation domain. This variation comes from two sources, firstly the particle analysed is positioned above a bounding layer of particles that will cause disruption of the channel flow especially at higher velocities. More significant however, is the motion of the particles as compared to a formulation designed to predict lift and drag on a stationary particle. Due to this, the simulation was revised and the top-most particle fixed such that steady state lift and drag forces could be obtained. Detail of these tests will be given in Section 4.1.2 where the simulated lift can be seen to match quite closely with Hele-Shaw relations at low flow rates.

*4.1.1. Grid Dependency Discussion*

Proof of concept testing was initially conducted at an LBM grid spacing of 1 $\mu m$. These results are not presented here, but they indicated that altering the Debye length around particles could alter the erosional properties of the system. However, to ensure that the hydrodynamic forces acting on the particles were grid-indepedent, this spacing was reduced to 0.5 $\mu m$. In order to keep the LBM relaxation parameter constant this doubling of resolution requires a factor of four reduction in the simulation time-step. Further details of the convergence study which guided the spacing used here can be found in Leonardi et al. (2013). Testing in this study indicated that the error in drag force for a particle mapped by four nodes could be expected to be on the order of 20%. With the increase to eight nodes (equivalent of 0.5 $\mu m$ spacing in this works) a reduction of error to approximately 4% is expected. This is relevant in Figure 10a where the steady-state simulation results closely match the predicted empirical drag force.

*4.1.2. Dislodgement Number Results*

In order to vary the hydrodynamic forces acting on the particles, the flow velocity was altered by applying different body forces to the simulation. In LBM, this is the equivalent of setting the pressure gradient across the domain. The six differentials tested were $0.1, 0.2, 0.4, 0.6, 0.8, 1.0\ Pa$. The resultant lift and drag forces are presented in Figure 10, showing that the drag aligns well with Hele-Shaw predictions, but the lift shows significant deviation. This is expected to be a result of the bounding particle layer and the choice of the empirical ($\chi$) coefficient in Equation 9. It is reported in Bedrikovetsky et al. (2011) that the value of this can vary between 89.5 and 1190 which can significantly alter the predicted behaviour of the system. This highlights the importance of a DNS approach in understanding the effects associated with empirical parameters.

Figure 11 plots the dimensionless dislodgement number from the values of lift and drag presented. It can be seen here that initially the fixed particle simulations very accurately predicted the value of the dislodgement number but deviate for higher flow rates. One of the causes of this is believed to be a result of the prediction of lift based on micro-channel flow relations in comparison with the effect of boundary particles as applied in simulation. Additionally, the empirical parameters used for Hele-Shaw lift and drag were taken from the works of Bedrikovetsky et al. (2011) where they were used to tune the developed model to a specific set of experimental results.

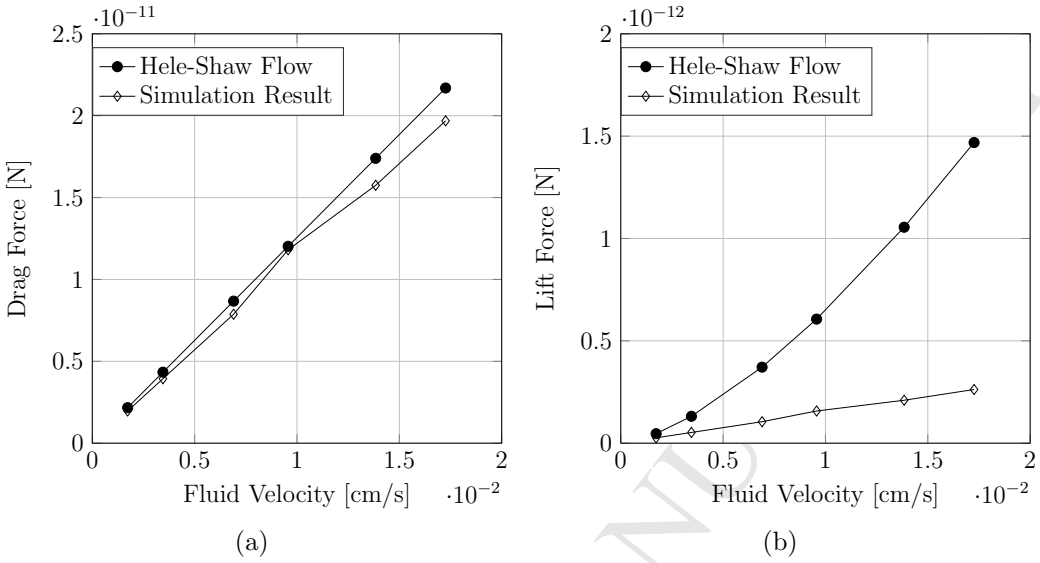


Figure 10: Results of fixed particle testing to obtain lift and drag forces in the investigation of dislodgement number, comparing fixed-simulation (a) drag ($\omega = 60$) and (b) lift ($\chi = 1190$) to the respective Hele-Shaw results.

The dislodgement numbers found as a result of the torque balance analysis appeared to give a reasonable match with simulation data. It was seen that the Hele-Shaw flow relations resulted in significantly larger predictions of steady state lift forces with the empirical coefficients used by Bedrikovetsky et al. (2011) and this impacted on the value of the dislodgement number quite substantially. However, it is noted that these empirical coefficients were given based on tuning to a particular set of experimental results that may have been taken under varying subsurface conditions.

The range of which the empirical coefficients were listed to be applicable by Bedrikovetsky et al. (2011) was between $10 \leq \omega \leq 60$ and $89.5 \leq \chi \leq 1190$. Figure 12 shows that $\chi = 250$ produces close alignment with the data obtained from direct numerical simulation of the physics described in this study.

It can be observed from altering the lift coefficient, $\chi$, that it is possible that the data used by Bedrikovetsky et al. (2011) to tune the fines migration model may have had differing electrostatic properties to those used in determining the DLVO force interactions. With further testing, it is expected that this method of determining the dislodgement number could be used based on

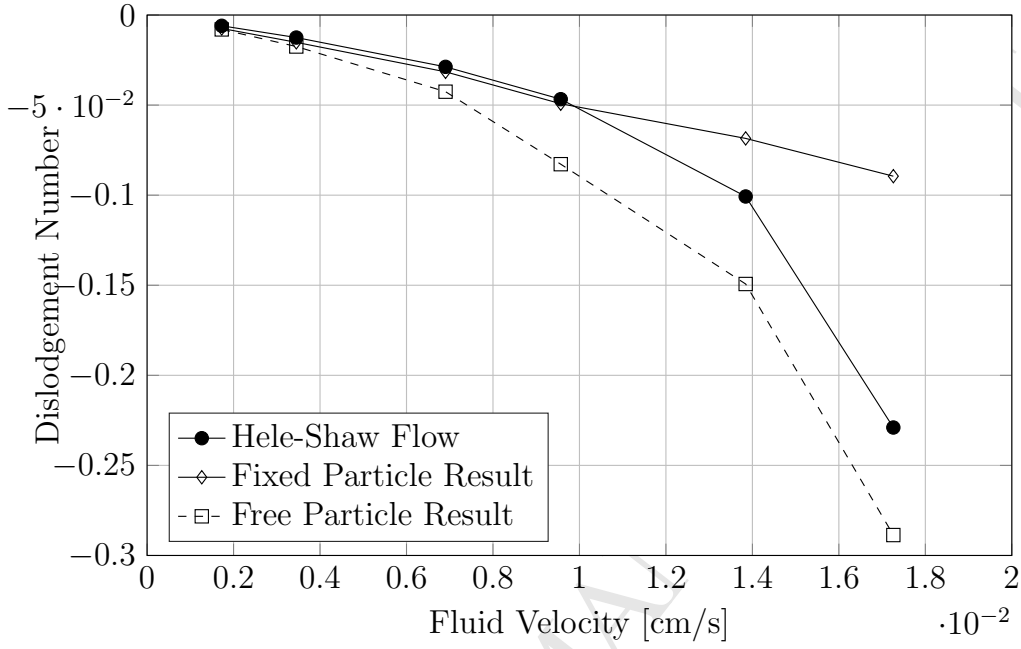


Figure 11: Comparison of the dislodgement number found from model results and theoretical formulations

the system properties (water salinity, zeta surface potentials etc.) in place of tuning to accumulated data. An additional note for further investigation is the horizontal motion of particles under low flow rates indicating possible limitations in the torque balance philosophy.

### *4.2. Preliminary Detachment Tests*

The previous test, although conducted in a 3D environment could effectively be analysed as a 2D system with negligible forcing in the z direction. Additionally, no analysis of moving particle interactions was undertaken, which has been referenced as a key behaviour in the migration of particles from the proximity of the bounding surface (Brumby et al. (2015)). Due to this, a simulation domain of size $40 \times 20 \times 10\ \mu m$ was constructed, again with wall conditions restricting the y-direction and periodic conditions in the x- and z-directions. From here a bounding particle layer was fixed and two free particles were initialised as seen in Figure 13. It is noted that due to the size of the particles (radius of 2 $\mu m$), and the resultant magnitude of the mass moment of inertia ($O(10^{-25})$ with density of 2650 $kg/m^3$), the rotational

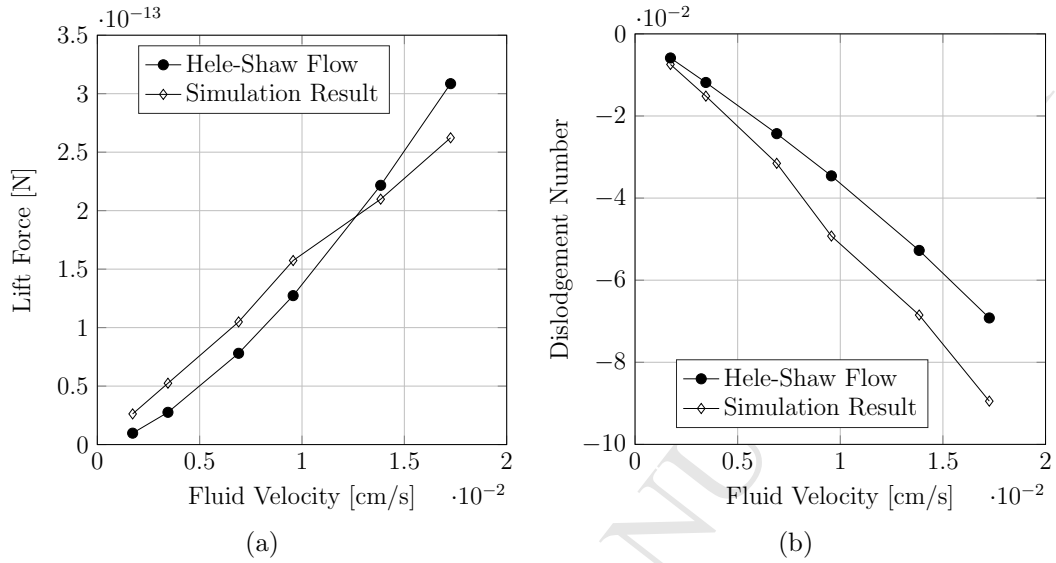


Figure 12: Tuning of empirical lift coefficient, $\chi$, as defined in the range specified by the literature, showing (a) force and (b) dislodging number as a function of fluid velocity for $\chi = 250$.

degrees of freedom were constrained to prevent non-physical fluctuations in angular velocity.

*4.2.1. Examination of the effect of lubrication forces*

As mentioned, the LBM is unable to accurately capture the momentum transfer between fluid and particles when surface separation is on the order of one cell spacing. Due to this, lubrication forces were implemented into the DEM framework and the effect of this on simulation results was determined. For this, a pressure gradient of 25 $Pa$ was applied across the domain which resulted in a maximum flow velocity of 1.443 $cm/s$ (this is achieved with a LBM body force of 500 $m/s^2$). For this section, DLVO parameters were held constant with values given in Table 5.

Figure 14 indicates that the lubrication forces act to reduce the predicted distance travelled by fine particles. Both simulations correctly captured the particle tumbling phenomena noted in other studies (Brumby et al., 2015). The particle rearrangement that occurs as a result appears similar to the motion of drafting-kissing-tumbling (DKT) seen in sedimentation. In the specific example tested here, the predicted particle migration distance when

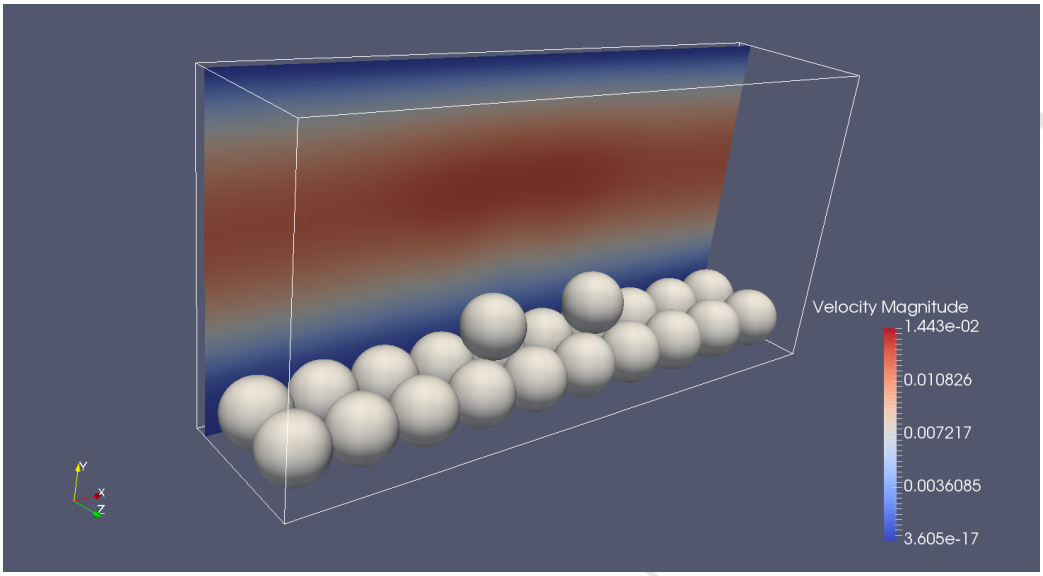


Figure 13: The layout of LBM-DEM simulations conducted for analysis of moving particle interaction, in which all particles are initially stationary.

neglecting lubrication forces was on average 65% larger than that found when these forces were incorporated. It is therefore evident that lubrication forces may have a significant impact on particle migration distances due to the proximity of particles during the erosion process.

*4.2.2. Examination of the effect of DLVO forces*

During the simulations, a set of both attractive (see Table 5) and repulsive DLVO parameters were used. These were achieved by varying the Debye length of the fluid by modelling salinity levels of 3000 $mg/L$ and 110 $mg/L$ respectively. These parameters were also used in simulations presented in Section 4.3.

Figure 15 shows a comparison of results under varied salinity levels with the same flow parameters as used in Section 4.2.1. Here it is evident that behaviours vary quite substantially between tests. It is noted through analysis of the Figure 15a, that under attractive conditions the particle tumbling behaviour (at approximately 0.01 *sec*) occurs at a higher rate as the two moving particles are forced together by the electrostatic interactions. This can be seen to cause larger displacements of the initially upstream particle that tumbles into the free stream flow. However, the downstream particle

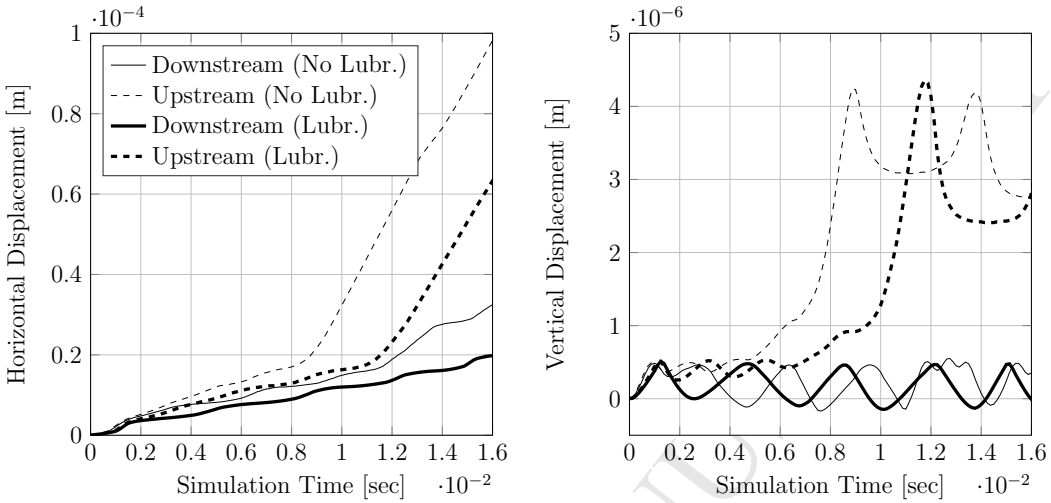


Figure 14: Comparison of the (a) horizontal and (b) vertical particle displacements observed in detachment tests with and without lubrication forces implemented.

Table 5: Base case DLVO parameters resulting in detachment tests with attractive conditions.

| Parameter | Nomenclature | Value | Units |
|---|---|---|---|
| *London-van der Waals:* | | | |
| Hamaker constant | $A_{132}$ | $2.02 \times 10^{-21}$ | $[J]$ |
| Diameter ratio | $y$ | 1 | $[-]$ |
| *Electric Double Layer:* | | | |
| Diameter ratio | $y$ | 1 | $[-]$ |
| Inverse Debye length | $k$ | $(6.05 \times 10^{-10})^{-1}$ | $[m^{-1}]$ |
| Surface potential | $\psi$ | $-30$ | $[mV]$ |

is forced towards the bounding surface the interaction where its motion is significantly reduced and electrostatic forces between the bounding surface become significant. Comparison of the displacement of the initially downstream particle allows one to conclude that for particles in close proximity to the bounding layer, attractive DLVO conditions (i.e. high salinity) result in a reduced displacement but the possibility for an increased rate of detrimental

interactions between moving particles.

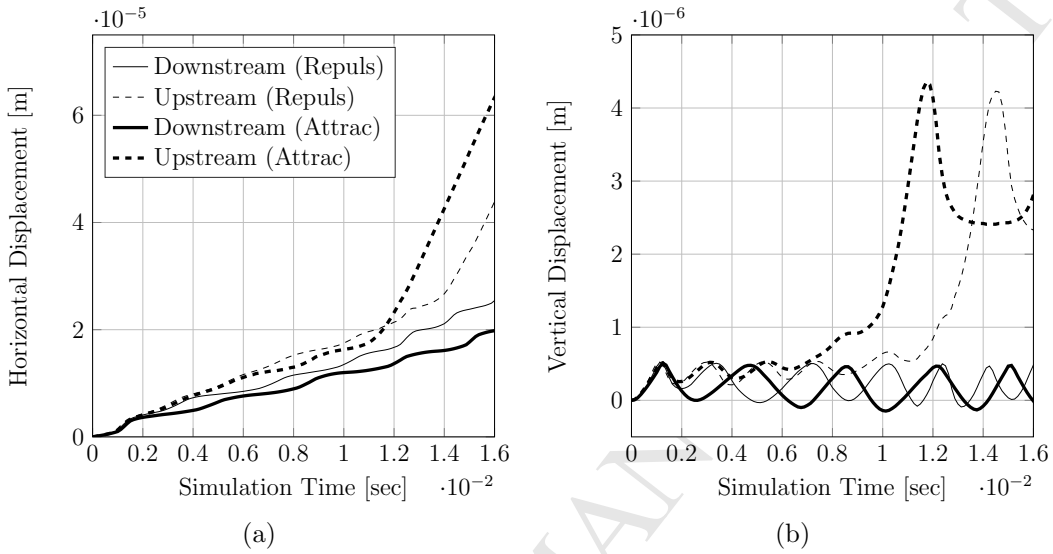


Figure 15: Comparison of the (a) horizontal and (b) vertical particle displacements observed in detachment tests under attractive and repulsive DLVO conditions.

It is observed in these tests that the hydrodynamic drag force dominates the electrostatic forces in the simulations. The ease with which the particles are moved is predicted to be amplified by the symmetry in the simulations conducted. The matching radius of fixed and free-to-move particles limits the mechanical resistance that would be present in a porous medium. This is neglected for the model development tests shown here, but future work will be aimed at randomly packed beds as well as the movement of these particles through samples scanned using microtomography.

During the tests it was observed that detached particles tended to follow the streamlines of the fluid with the lift force not sufficient to propel particles into the free stream. This indicated that some other phenomena must occur in order to separate the particles from the bounding surface. As simulations progressed, the phenomenon of particle tumbling was seen. This can be described as a similar motion to that of DKT type behaviour, and aligns with the findings of Brumby et al. (2015). Figure 16 shows the interaction of two moving particles, where the rolling motion causes a significant vertical displacement of the faster moving particle. In this case the tumble causes the initially downstream particle to be displaced into the region of slow flow

near the boundary while projecting the upstream particle further into the free stream.

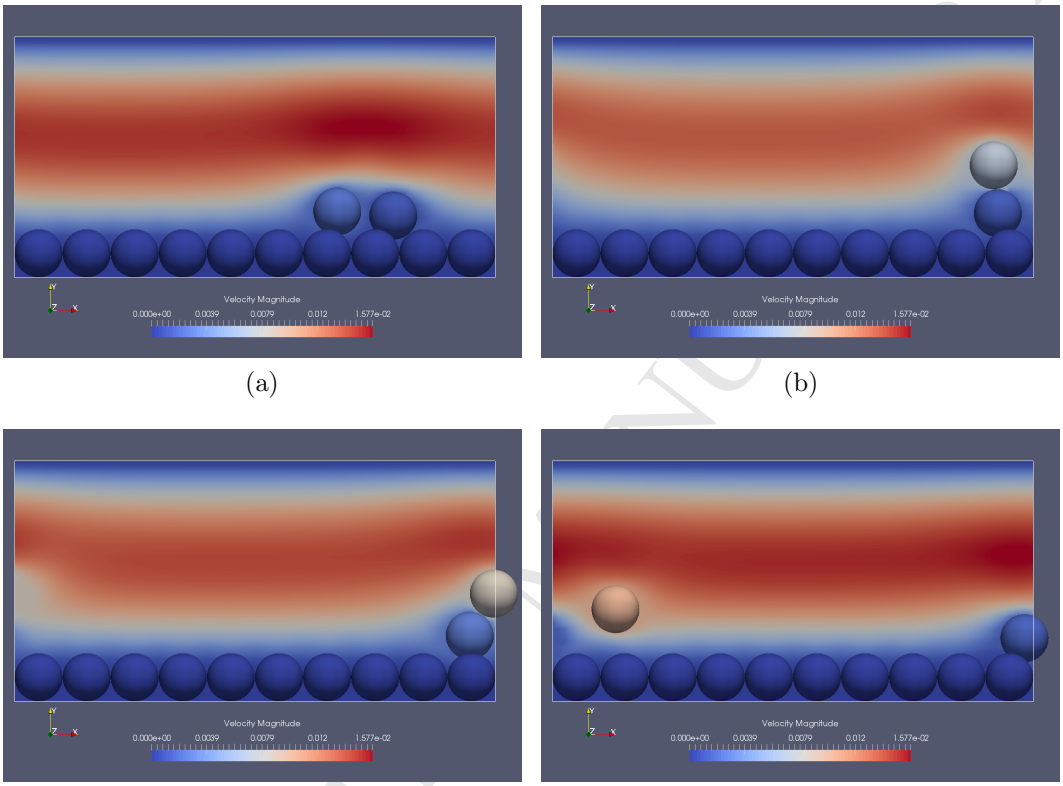


Figure 16: The particle rearrangement observed which seems similar to the effect of a drafting-kissing-tumbling (DKT) interaction, highlighting (a) particle approach, (b) post-interaction as tumbling begins, (c) particle tumbling, and (d) the post-tumbling configuration.

From this LBM-DEM simulation domain, it was shown that lubrication forces play an important role in the interaction of fines. Additionally, it was seen that the computational model was capable of capturing physical phenomena such as particle tumbling. It was evident that this behaviour was also required to detach particles into the free stream flow. Therefore, this initial LBM-DEM phase has indicated that not only electrostatic conditions can alter the migration rates of fines, but that the model is capable of capturing physically recognised phenomena.

*4.3. Fines Migration Testing*

Using the insights gained from initial detachment tests, simulations were constructed to investigate the liberation process in greater detail. These consisted of multi-layered particles packed in a face-centred cubic array. The bottom layer was fixed to act as a bounding surface and mimic a deep particle layer. An intermediary layer of free-to-move particles was packed onto the bounding layer and a sparse top layer was superimposed on this. The physical domain size was $32 \times 16 \times 15$ $\mu m$ with the LBM grid spacing and time step as previously specified. Particle sizing was consistent with preliminary tests where a 2 $\mu m$ radius was used. The LBM domain was periodic in the x- and y-directions, but the height of the domain in the z-direction was restricted by wall boundary conditions.

Figure 17 shows the initial testing domain constructed for liberation simulations. The aim of this simulation was to show on a larger scale the general behaviour of the colloidal fines and determine the effect of varied flow conditions. Primary analysis of this test domain focused on the attractive conditions predicted to occur in a coal seam-like environment. However, comparative tests were conducted in a repulsive environment as an indication of how altering the Debye length around particles can influence the detachment of fines.

In order to quantitatively compare tests of varying flow velocities and electrostatic conditions, erosion amounts and rates were defined. This is done by determining the amount of mass liberated above a specified $x - y$ plane within the domain, located to align with the topmost initialised particle at a height of 9.75 $\mu m$. Measuring the amount of mass above this plane allowed the erosion rate, $E$ $[kg/sm^2]$, to be defined as,

$$E = \frac{\Delta m}{A_{xy} \Delta t}, \tag{28}$$

where $\Delta m$ is the change of mass above the plane from the previous time step, $A_{xy}$ is the cross-sectional area of the plane and $\Delta t$ is the time step of the simulation (Brumby et al., 2015).

Figure 18 indicates the positioning of the erosion plane and shows how particles gradually propagate above it as they tend away from the bounding surface. From here, the volume of solid phase above the plane is determined and an eroded mass quantity is found. The results obtained for each flow

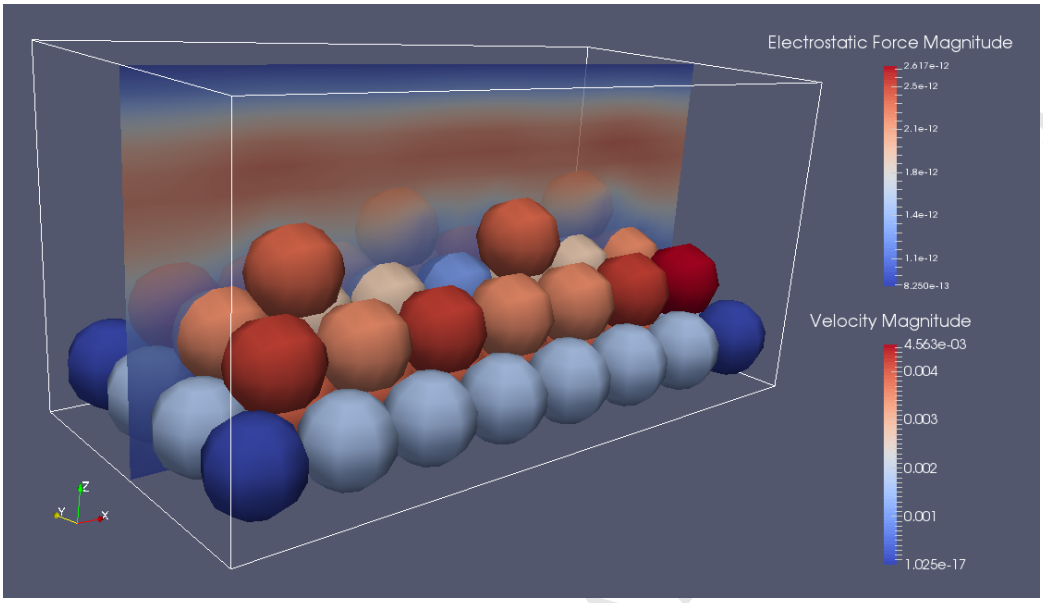


Figure 17: The layout of LBM-DEM simulations conducted for liberation testing. The particle colouring is indicative of electrostatic force [N] while the fluid is coloured based on flow velocity [m/s].

condition tested under attractive DLVO conditions can be seen in Table 6. Here, erosion rates for applied pressure gradients agreed well with the results of Brumby et al. (2015). To show the erratic nature of erosion, the mass at each time step above the specified $x - y$ plane is given in Figure 19.

Table 6: Erosion results from liberation testing under attractive DLVO conditions.

| $\Delta$Pressure $[Pa]$ | Avg. Max. Flow $[m/s]$ | Eroded Mass $[kg]$ | Erosion Rate $[kg/m^2s]$ |
|---|---|---|---|
| 1.5 | 0.000329 | 1.6223E-14 | 0.00095 |
| 3.0 | 0.000621 | 5.24498E-15 | 0.00031 |
| 4.5 | 0.001043 | 4.76826E-14 | 0.00279 |
| 7.5 | 0.001581 | 2.70001E-14 | 0.00158 |
| 15.0 | 0.003102 | 6.97355E-14 | 0.00409 |
| 75.0 | 0.0151700 | 2.12208E-13 | 0.012434 |

In order to gauge the impact of the electrostatic interaction between colloidal particles, liberation tests were additionally performed under the repulsive conditions used in Section 4.2.2. This was completed for all pressure

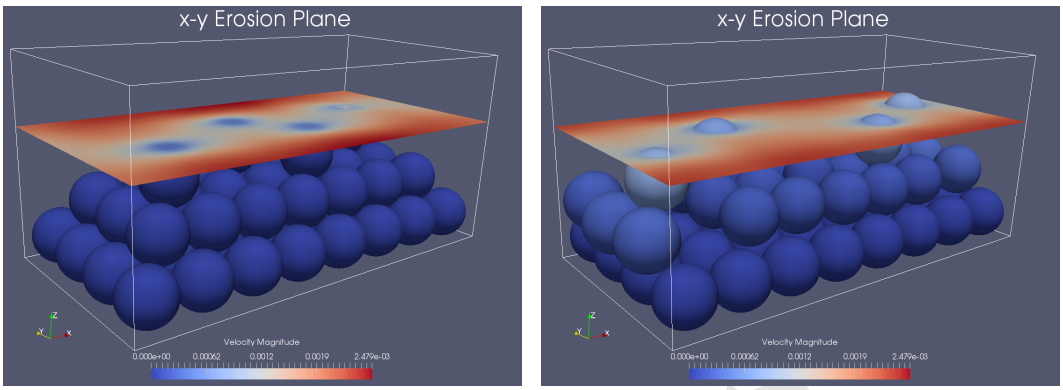


(a) (b)

Figure 18: Positioning of the erosion plane for liberation tests at (a) the commencement of simulations and (b) during the final time step of a simulation with an applied pressure difference of 7.5 $Pa$.

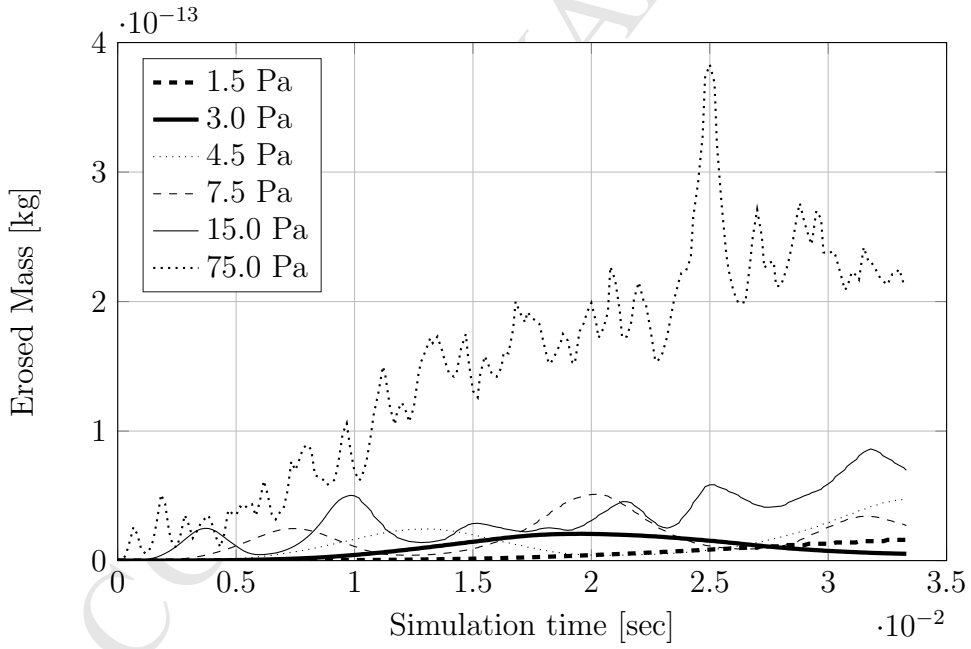


Figure 19: Results of liberation tests showing the eroded mass over time for varied flow conditions.

gradients tested under attractive conditions. Figure 20 shows the time com-

parison of the simulation run with $\Delta P = 7.5\ Pa$ and indicates the earlier onset of erosion due to the electrostatic repulsion of particles. The final erosion rate calculated in this case was found to be 0.003535 $kg/m^2s$. This indicates a 123% increase in both the amount of mass eroded and resultant erosion rate due to the change in electrostatic properties. Table 7 shows a comparison of the influence of the electrostatic force with varied flow rates. Here an outlier is observed when a pressure gradient of 3 $Pa$ is applied and this is believed to be a result of the particles initial positions, however in general it can be seen that DLVO parameters have a significant impact on the erosion properties of this idealised test case.

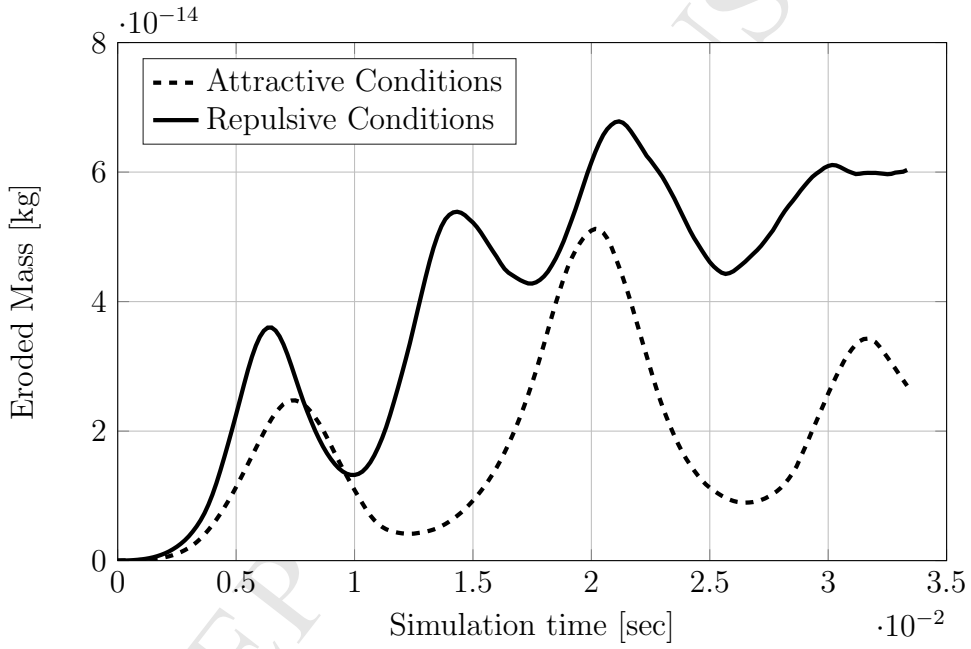


Figure 20: Comparison of varying DLVO parameters for attractive and repulsive conditions in particle liberation tests with a pressure differential of 7.5 $Pa$.

These results look towards a proof of concept in which altering electrostatic forces in the subsurface environment could be used to reduce the migration of fine particles. Figure 21 shows the again erratic nature of erosion results. This is likely to be a result of scaling, in which each particle that moves above the erosion plane has a significant impact on the total eroded mass. This issue could be overcome with larger simulations, which is one avenue of future research.

Table 7: Comparison of erosion rates determined under varying electrostatic conditions.

| $\Delta$P $[Pa]$ | Attractive Erosion Rate $[kg/m^2s]$ | Repulsive Erosion Rate $[kg/m^2s]$ | Percent Increase |
|---|---|---|---|
| 1.5 | 9.51E-04 | 2.53E-03 | 166 |
| 3.0 | 3.07E-04 | 3.08E-03 | 901 |
| 4.5 | 2.79E-03 | 3.81E-03 | 36 |
| 7.5 | 1.58E-03 | 3.54E-03 | 123 |
| 15.0 | 4.09E-03 | 4.43E-03 | 9 |
| 75.0 | 1.24E-02 | 1.43E-02 | 15 |

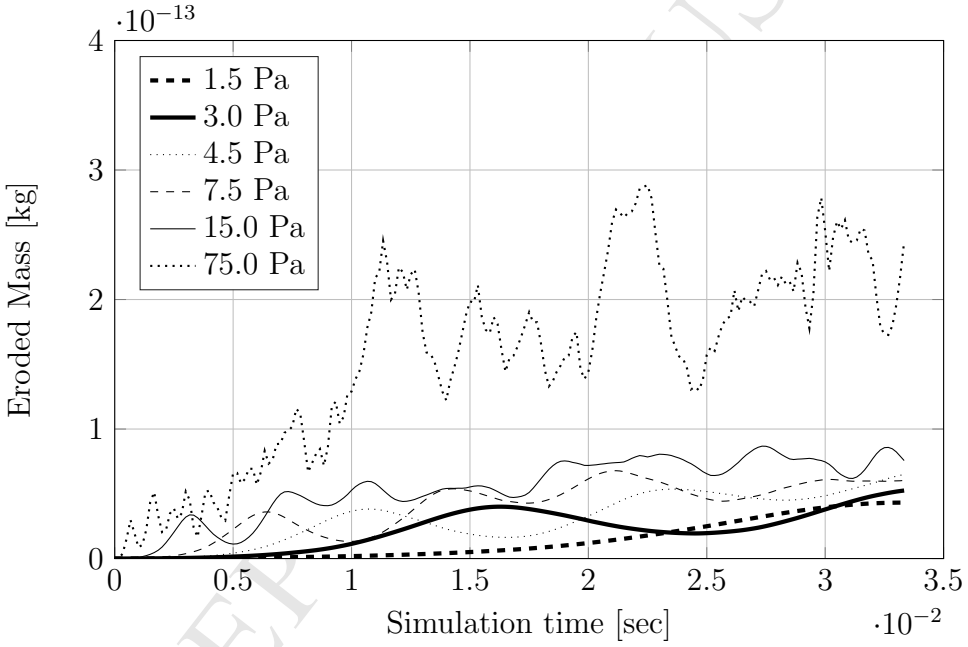


Figure 21: Results of liberation tests under repulsive electrostatic conditions showing the eroded mass over time.

During testing, the sliding of colloidal particles along the fixed boundary was evident. In order to study this phenomenon, the size of free to move particles was reduced to increase the mechanical resistance possible from the bounding surface. Figure 22 indicates the new layout of particles, a face-centred cubic array is still used but free particles are randomly sized with radii of $1 \pm 0.5$ $\mu m$. This involved adapting the packing algorithm

to randomly assign particle radii within the given bounds in an attempt to create increased particle capture positions. It is noted that this reduction in particle size with constant LBM grid spacing can impact the accuracy of hydrodynamic force calculations, but this is deemed acceptable for this test case. In altering the particle radii, the mechanical resistance in the direction of flow is increased as particles can more easily become lodged in gaps within the bounding surface. To assess the effect of this in comparison with the uniform particle size test cases, a pressure gradient of 15 $Pa$ was applied across the domain, and the erosion amount and rate was determined.

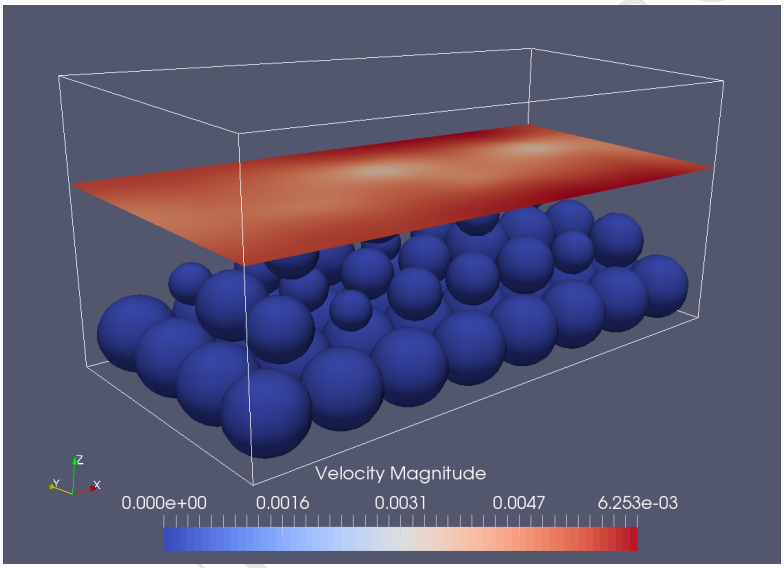


Figure 22: The arrangement of LBM-DEM simulations of particle liberation tests using varied particle sizes.

Figure 23 provides a comparison of the eroded mass over time for these two test cases. Here it is clear that the rate at which particles are able to move away from the bounding surface is significantly reduced for randomly sized particles. With the smaller particles more easily captured in gaps within the bounding surface, the erosion rate drops 58.4% from 0.00409 to 0.00170 $kg/m^2s$. A further test of this property would be to initialise a randomly packed distribution of particles with an equivalent void fraction to the uniformly distributed particles cases conducted in this work. This presents another possible avenue for future work.

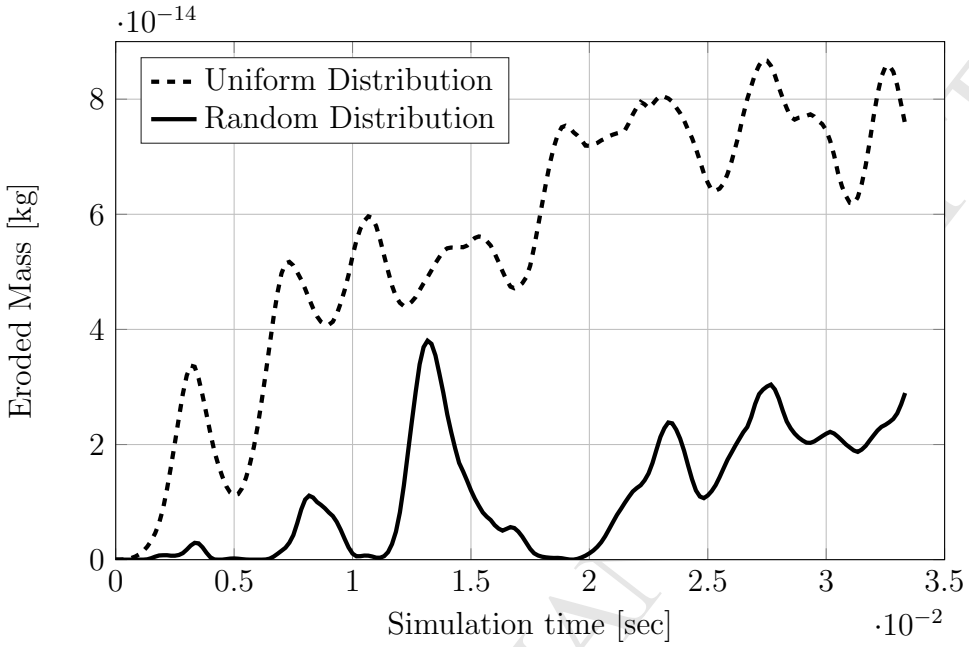


Figure 23: Comparison of the eroded mass during the uniform and randomised radius tests of particle liberation.

*4.3.1. Fines Migration Discussion*

During this testing phase, flow velocities of 0.03 $cm/s$ to 1.5 $cm/s$ were observed with each recorded to have caused erosion of mass to some degree. This is in line with preliminary results that found particle movement for all flow rates tested. It is noted that the majority of tests were conducted at flow rates under 0.3 $cm/s$ with one higher flow test performed to assess the behaviour of fines under a regime dominated by hydrodynamic forces.

The notable sliding of particles over the lower layers brings to question whether all the mass above the plane is truly eroded or a result of a high point in the bounding layer. It was decided in the works of this study that defining the erosion plane as stated was sufficient. It not only aligned with similar investigations in literature, but the increasing trends seen in all erosion simulations indicate the fluctuations due to sliding particles are negligible over the length of a simulation.

Figure 24 was produced from data presented in Table 7. This was conducted to further study the erosion rates defined at the end of each liberation test. Here it is seen that with all simulation parameters constant except for

the Debye length, a significant effect on erosion is evident. Large variations at low velocities are expected here with minimal lift force resulting in the dominance of electrostatic forces. Under these conditions, attractive DLVO forces act to resist particle motion away from the bounding layer resulting in reduced erosion rates.

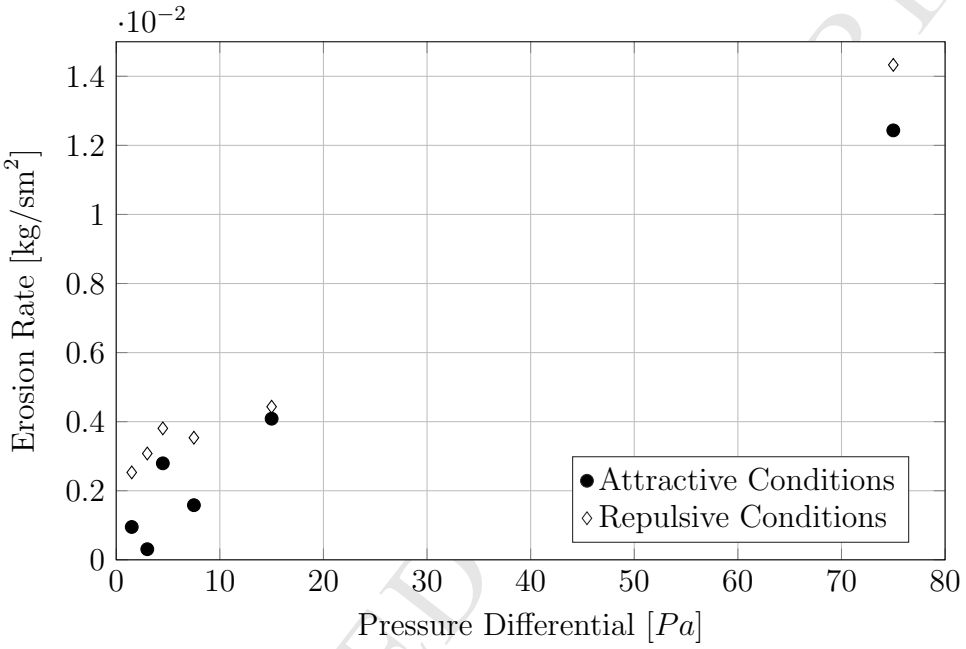


Figure 24: Analysis of erosion rates under attractive and repulsive conditions for varying pressure gradients.

With a particular focus on the effect of DLVO conditions, it was hypothesised from preliminary tests that increased displacement would occur for particles close to the bounding surface under repulsive conditions resulting in an increased rate of erosion. The preliminary detachment tests indicated approximately a 30% variation in travelled distance with flow velocities of the order of 1.4 $cm/s$, and as such relatively large variations were expected in erosion tests. It was observed, that the repulsive parameters defined caused an increased erosion rate for all tests, but did not follow a simple trend. This is believed to be a result of the noise involved in measuring the eroded mass with small-scale simulations, here each eroded particle has a significant contribution to the erosion rate and as such each measurement has a degree of time dependency. In assessing the variation of erosion with altered electro-

static conditions however, these results clearly indicate the potential for use in minimising the production of fines from the subsurface environment.

The impact of this result on CSG fines migration is the ability to simulate varying subsurface conditions and report on the resultant erosional behaviour. Various suggestions exist for how the electrostatic properties could be controlled. Of particular note is the use of nanoparticles as described by Assef et al. (2014) and Arab et al. (2014). It was noted that repulsive electrostatic behaviour was created in test cases presented in this work by altering the Debye length in the electric double layer formulation. Preliminary sensitivity testing indicated that increased attractive or repulsive conditions could also be obtained by altering the zeta potential (related to surface charge) of the particles. Using this idea, nanoparticle solutions are able to alter the effective potential to obtain favourable conditions for retention or detachment. In order to reduce the fines released and improve capture of suspended fines, nanoparticles such as magnesium oxide (MgO) have been tested and found to reduce the effect of the electric double layer (Assef et al., 2014). The development of the erosional framework constructed inside of the presented code could be applied as a preliminary assessment tool to predict the effects these solutions have on the subsurface environment.

## 5. Concluding Remarks

Coal seams have becoming an important source of natural gas. Deleterious processes such as fines migration can severely decrease reservoir permeability and cause equipment failure, both down-hole and on the surface, and need to be resolved to assist economical production. In order to mitigate the effects of fines migration, an understanding of the physical interactions involved must first be developed. In this paper, direct numerical simulation on the grain-scale was utilised to ascertain how fines interact amongst each other and with production fluid during the dewatering stage of a well.

The investigation that was undertaken focused on the development of an explicit numerical model to study the electrostatic interactions between colloidal particles. The model was based on a pre-existing coupled LBM-DEM framework, in which the LBM was used to replicate fluid and the DEM to capture particle trajectories. The primary addition to this framework has been the incorporation of DLVO interactions, smaller developments such as random particle sizing and variable pressure gradients have also been made.

Theoretical sensitivity analysis of DLVO parameters demonstrated the potential conditions required for overall repulsive or attractive particle behaviour. In simulation testing a repulsive environment was created through adjustment of the Debye length by reducing the fluid salinity. This effects the length over which the electric double layer diffuses. The comparison of conditions showed that reduced fines migration velocities and erosion parameters are found in an attractive electrostatic environment.

In liberation testing, erosion was defined as the movement of mass above a specified plane. With this definition, total eroded mass and erosion rates were defined for varying flow velocities. An almost linear trend between pressure gradient and fines migration was observed throughout testing. It is noted that in these tests, a critical velocity below which no erosion occurs was not observed as mentioned by Brumby et al. (2015). This is believed to be a result of increased simulation run times used in this work as well as the symmetric face-centred cubic packed array and the uniform particle sizing providing minimal mechanical resistance in the direction of flow. Introduction of varied particle radius saw an immediate drop in erosion rates as additional force was required to propagate free-to-move particles over the boundary. Extension of this to random packing is hypothesised to demonstrate a critical flow rate prior to which negligible erosion is generated.

This study aimed at providing a robust framework for implementation into large-scale studies. Throughout the course of the investigations, opportunities for further work were noted. From the significant variation of results in randomised particle size testing, it would be desirable to simulate randomly packed particles for which a solid volume fraction could be defined. Additionally, the interaction of complex geometries could lead to larger mechanical resistance to detachment and alter the erosional behaviour of the system. The physicochemical properties may also change over time in a realistic scenario, and the ability to replicate this would also be useful. This could then be utilised to show the effect of operations such as pumping nanoparticle-laden fluid in order to alter particle surface potentials. Finally, the simulations presented here are limited to a single fluid phase so to capture behaviour of the reservoir at later stages of development extension to multiphase fluid flow would be required.

**Acknowledgements**

The authors would like to thank Prof. Pavel Bedrikovetski for his many helpful observations during the preparation of this manuscript.

**References**

Aidun, C. K., Clausen, J. R., 2010. Lattice-Boltzmann method for complex flows. Annual Review of Fluid Mechanics 42 (1), 439–472.

Aidun, C. K., Lu, Y., Ding, E.-J., 2000. Direct analysis of particulate suspensions with inertia using the discrete Boltzmann equation. Journal of Fluid Mechanics 373 (-1), 287–311.

Al-Abduwani, F., Bedrikovetsy, P., Farajzadeh, R., van den Broek, W., Currie, P., 2005. External filter cake erosion: Mathematical model and experimental study. Society of Petroleum Engineers, Paper no. 94635.

Arab, D., Pourafshary, P., Ayatollahi, S., 2014. Mathematical modeling of colloidal particles transport in the medium treated by nanofluids: Deep bed filtration approach. Transport in Porous Media 103 (3), 401–419.

Assef, Y., Arab, D., Pourafshary, P., 2014. Application of nanofluid to control fines migration to improve the performance of low salinity water flooding and alkaline flooding. Journal of Petroleum Science and Engineering 124, 331 – 340.

Bedrikovetsky, P., Siqueira, F., Furtado, C., Souza, A., 2011. Modified particle detachment model for colloidal transport in porous media. Transport in Porous Media 86 (2), 353–383.

Bhatnagar, P. L., Gross, E. P., M., K., 1954. A model for collision processes in gases. i. small amplitude processes in charged and neutral one-component systems. Physical Review 94 (3), 511–525.

Bradford, S. A., Simunek, J., Bettahar, M., van Genuchten, M. T., Yates, S. R., 2003. Modeling colloid attachment, straining, and exclusion in saturated porous media. Environmental Science & Technology 37 (10), 2242–2250.

Bradford, S. A., Torkzaban, S., 2008. Colloid transport and retention in unsaturated porous media: A review of interface-, collector-, and pore-scale processes and models. Vadose Zone Journal 7 (2), 667.

Brumby, P., Sato, T., Nagao, J., Tenma, N., Narita, H., 2015. Coupled LBM-DEM micro-scale simulations of cohesive particle erosion due to shear flows. Transport in Porous Media 109 (1), 43–60.

Chen, S., Doolen, G. D., 1998. Lattice Boltzmann method for fluid flows. Annual Review of Fluid Mechanics 30 (1), 329–364.

Chun, B., Ladd, A. J. C., 2007. Interpolated boundary condition for lattice Boltzmann simulations of flows in narrow gaps. Physical Review E 75 (6), 066705–12.

Cook, B. K., Noble, D. R., Williams, J. R., 2004. A direct simulation method for particle-fluid systems. Engineering Computations 21 (2/3/4), 151–168.

Cundall, P. A., Strack, O. D. L., 1979. A discrete numerical model for granular assemblies. Geotechnique 29 (1), 47–65.

Daintith, J., 2008. A dictionary of chemistry, 6th Edition. Oxford University Press.

Ding, E.-J., Aidun, C. K., 2003. Extension of the lattice-Boltzmann method for direct simulation of suspended particles near contact. Journal of Statistical Physics 112 (3), 685–708.

Hamaker, H. C., 1937. The London-van der Waals attraction between spherical particles. Physica 4 (10), 1058–1072.

Han, K., Peric, D., Crook, A. J. L., Owen, D. R. J., 2000a. A combined finite/discrete element simulation of shot peening processes - Part I: studies on 2D interaction laws. Engineering Computations 17 (5), 593–619.

Han, K., Peric, D., Owen, D. R. J., Yu, J., 2000b. A combined finite/discrete element simulation of shot peening processes - Part II: 3D interaction laws. Engineering Computations 17 (6), 680–702.

Khilar, K. C., Fogler, H. S., 1998. Migrations of Fines in Porous Media. Springer Netherlands.

Kim, S., Karrila, S. J., 1991. Microhydrodynamics: principles and selected applications. Butterworth-Heinemann, Boston.

Ladd, A. J. C., 1994a. Numerical simulations of particulate suspensions via a discretized Boltzmann equation. part 1. theoretical foundation. Journal of Fluid Mechanics 271, 285–309.

Ladd, A. J. C., 1994b. Numerical simulations of particulate suspensions via a discretized Boltzmann equation. part 2. numerical results. Journal of Fluid Mechanics 271, 311–339.

Leonardi, C., Jones, B., Holmes, D., Williams, J., 2013. Simulation of complex particle suspensions using coupled lattice Boltzmann-discrete element methods. 6th International Conference on Discrete Element Methods (DEM6), Golden.

Leonardi, C. R., Owen, D. R. J., Feng, Y. T., 2012a. Simulation of fines migration using a non-Newtonian lattice Boltzmann-discrete element model part i: 2D implementation aspects. Engineering Computations 29 (4), 366–391.

Leonardi, C. R., Owen, D. R. J., Feng, Y. T., 2012b. Simulation of fines migration using a non-Newtonian lattice Boltzmann-discrete element model Part ii: 3D extension and applications. Engineering Computations 29 (4), 392–418.

Liang, Y., Hilal, N., Langston, P., Starov, V., 2007. Interaction forces between colloidal particles in liquid: Theory and experiment. Advances in Colloid and Interface Science 134-135 (0), 151 – 166, topical issue in honour of Victor Starov.

Lomin, F., Scholts, L., Sibille, L., Poullain, P., 2013. Modeling of fluid-solid interaction in granular media with coupled lattice Boltzmann-discrete element methods: application to piping erosion. International Journal for Numerical and Analytical Methods in Geomechanics 37 (6), 577–596.

McNamara, G. R., Zanetti, G., 1988. Use of the Boltzmann equation to simulate lattice-gas automata. Physical Review Letters 61 (20), 2332–2335.

Nguyen, N.-Q., Ladd, A. J. C., Oct 2002. Lubrication corrections for lattice-Boltzmann simulations of particle suspensions. Phys. Rev. E 66, 046708.

Noble, D. R., Torczynski, J. R., 1998. A lattice-Boltzmann method for partially saturated computational cells. International Journal of Modern Physics C 9 (8), 1189–1201.

Pan, C., Luo, L.-S., Miller, C. T., 2006. An evaluation of lattice Boltzmann schemes for porous medium flow simulation. Computers & Fluids 35 (8-9), 898–909, proceedings of the First International Conference for Mesoscopic Methods in Engineering and Science.

Ryan, J. N., Elimelech, M., 1995. Colloid mobilization and transport in groundwater. Colloids and surfaces. A, Physicochemical and Engineering Aspects 107, 1–56.

Sane, J., 2005. Effect of brownian forces and hydrodynamic iinteraction on ccolloid in confined flows. Master's thesis, University of Cambridge.

Semwogerere, D., Morris, J. F., Weeks, E. R., June 2007. Development of particle migration in pressure-driven flow of a Brownian suspension. Journal of Fluid Mechanics 581, 437.

Sterling, J. D., Chen, S., 1996. Stability analysis of lattice Boltzmann methods. Journal of Computational Physics 123 (1), 196–206.

Succi, S., 2001. The lattice Boltzmann equation for fluid dynamics and beyond. Oxford University Press.

Verberg, R., Ladd, A. J. C., 2000. Lattice-Boltzmann model with sub-grid-scale boundary conditions. Physical Review Letters 84 (10), 2148–2151.

Verberg, R., Ladd, A. J. C., 2001. Accuracy and stability of a lattice-Boltzmann model with subgrid scale boundary conditions. Physical Review E 65 (1), 1–16.

Williams, J. R., O'Connor, R., 1999. Discrete element simulation and the contact problem. Archives of Computational Methods in Engineering 6 (4), 279–304.

Zeinijahromi, A., Vaz, A., Bedrikovetsky, P., Borazjani, S., 2012. Effects of fines migration on well productivity during steady state production. Journal of Porous Media 15 (7), 665–679.

Zhang, J.-F., Zhang, Q.-H., 2011. Lattice Boltzmann simulation of the flocculation process of cohesive sediment due to differential settling. Continental Shelf Research 31, 94–105.

***Highlights:***

- A coupled LBM-DEM model was developed to simulate particle liberation in coal seams
- Physicochemical interactions were adjusted to inhibit or assist fines detachment
- Mechanism for free-stream detachment was found to rely on particle-particle tumbling
- Simulation upscaling and random particle packing to be investigated in the future